

Acquisitions and Bibliographic Services Branch

395 Wellington Street Ottawa, Ontario K1A 0N4 Bibliothèque nationale du Canada

Direction des acquisitions et des services bibliographiques

395, rue Wetlington Ottawa (Ontario) K1A 0N4

Your Ne Voire reférence

Out Me. Notre référence

NOTICE

The quality of this microform is heavily dependent upon the quality of the original thesis submitted for microfilming. Every effort has been made to ensure the highest quality of reproduction possible.

If pages are missing, contact the university which granted the degree.

Some pages may have indistinct print especially if the original pages were typed with a poor typewriter ribbon or if the university sent us an inferior photocopy.

Reproduction in full or in part of this microform is governed by the Canadian Copyright Act, R.S.C. 1970, c. C-30, and subsequent amendments.

AVIS

La qualité de cette microforme dépend grandement de la qualité de la thèse soumise au microfilmage. Nous avons tout fait pour assurer une qualité supérieure de reproduction.

S'il manque des pages, veuillez communiquer avec l'université qui a conféré le grade.

La qualité d'impression de certaines pages peut laisser à désirer, surtout si les pages originales ont été dactylographiées à l'aide d'un ruban usé ou si l'université nous a fait parvenir une photocopie de qualité inférieure.

La reproduction, même partielle, de cette microforme est soumise à la Loi canadienne sur le droit d'auteur, SRC 1970, c. C-30, et ses amendements subséquents.

ll

Canadä^{*}

Design and Characteristics of a General Purpose Atomic Force Microscope

Philip R. LeBlanc
Department of Physics, McGill University
Montréal, Québec

A Thesis submitted to the
Faculty of Graduate Studies and Research
in partial fulfillment of the requirements for the degree of
Master of Science in physics

© Philip R. LeBlanc, 1996



Acquisitions and Bibliographic Services Branch

395 Wellington Street Ottawa, Ontario K1A 0N4 Bibliothèque nationale du Canada

Direction des acquisitions et des services bibliographiques

395, rue Wellington Ottawa (Ontario) K1A 0N4

Your file Votre référence

Our file Notre référence

The author has granted an irrevocable non-exclusive licence allowing the National Library of Canada to reproduce, loan, distribute or sell copies of his/her thesis by any means and in any form or format, making this thesis available to interested persons.

L'auteur a accordé une licence irrévocable et non exclusive permettant à la Bibliothèque nationale dи Canada reproduire, prêter, distribuer ou vendre des copies de sa thèse de quelque manière et sous quelque forme que ce soit pour mettre des exemplaires de cette thèse disposition la des personnes intéressées.

The author retains ownership of the copyright in his/her thesis. Neither the thesis nor substantial extracts from it may be printed or otherwise reproduced without his/her permission. L'auteur conserve la propriété du droit d'auteur qui protège sa thèse. Ni la thèse ni des extraits substantiels de celle-ci ne doivent être imprimés ou autrement reproduits sans son autorisation.

ISBN 0-612-12221-2



CONTENTS

	RÉ	SUMÉ	iii
	ABSTRACT		
	Acknowledgments		
_		v	
1 Introduction			2
2	Introduction to Scanning Force Microscopy		4
	2.1	Forces	8
		2.1.1 Van der Waals Forces	8
		2.1.2 Electrostatic Forces	8
		2.1.3 Magnetic Forces	10 12
	2.2	Force Sensors	14
	2.3	Deflection Sensors	16
	2.0	2.3.1 Interferometry	18
	2.4	Piezoelectrics and their Associated Nonlinearities	19
		2.4.1 Hysteresis	20
		2.4.2 Greep	21
		2.4.3 Cross Coupling	22
	2.5	Other Artifacts	23
	2.6	All is not lost	24
3 MICROSCOPE DESIGN AND CHARACTERISTICS		CROSCOPE DESIGN AND CHARACTERISTICS	25
Ī	3.1	General Design	25
	3.2	Sample Scanner	31
	3.3	Fiber Optic Interferometer	34
	3.4	Vibration Damping and Noise	35
	3.5	Electrical Connections to Microscope	45
	3.6	Electromagnet	50
	3.7	Data Analysis	54
4	Co	ONCLUSION	56
5 Impovements and Suggestions			57
•	5.1	Improvements	57
	5.2	Suggestions	58
	_	PENDICES	59
		Data Transfer from PC to INDY	59
		PV-WAVE	60
		SXM	63
	-	Other Noise Sources	63
		FERENCES	65

RÉSUMÉ

Une nouvelle classe de microscope, le microscope à effet force (MEF), nous permet de mieux investiguer le monde atomique. Notre groupe à l'université McGill a développé un MEF qui nous permet d'obtenir des images, de faire de la spectroscopie et même de manipuler des échantillons à l'échelle atomique.

Nous avons dû surmonter plusieurs défis lors de la construction de ce microscope. Pour isoler le système des vibrations, par exemple celles du bâtiment et des gens qui marchent et parlent près du microscope, nous avons développé un système d'isolation qui inclut une série de plaques de métal qui supporte le microscope.

Pour étudier les propriétés magnétiques d'un échantillon, nous avons construit un électro-aimant avec un champ magnétique de 1 kiloGauss. L'aimant est facile à contruire et pourra être utilisé *in situ* pour changer l'aimantation des échantillons.

ABSTRACT

A powerful new class of microscope, the Atomic Force Microscope, has led to a deeper understanding of the nanoscale world. The Scanning Probe Microscopy group at McGIII University has developed an AFM whose general design lends itself readily to imaging, spectroscopy, and manipulation on an atomic scale.

There are many challenges to building such a system. A major concern is the isolation of the microscope from external vibration sources, such as building vibration, people walking and talking next to the microscope, etc. These vibrations are orders of magnitude larger than the precision needed to detect the small variations of an atomic surface. A number of measures were developed to provide the isolation needed, including a series damping plates that support the microscope.

An electromagnet was developed as an addition to the microscope as an aid to investigate the magnetic properties of samples. The magnet design combines a maximum magnetic field of over 1 kiloGauss with a simple construction and wire winding. Using this magnet, we will be able to rotate sample magnetizations in situ to observe switching times and profiles.

ACKNOWLEDGMENTS

I would like to thank a number of people without whom this work would not have been possible, nor as fun.

Huge thanks go out to my parents, Denyse and Robert, for their teachings, their generosity and their love. Thanks also to my brother, Alex, for not strangling me the year he got bigger than me.

I thank all of my friends for their, well, friendship. In particular I thank Anne Marie for her understanding, Rebecca for all the fun, Chris for being so incredibly in tune with my psyche and my stomach, Dan for the Monty Python, Colin and Liz for the signing, Christine, Jean-François, Stéphane and Réjean for the tarot, Lisa, Lysa, Samantha and Lisa for the dancing, May and James for being the sweetest couple I know, Eric for the squash games and Melinda for my soul.

I'd also like to thank my collegues, Yanzhang, Graham, and Mark for our discussion and their patient explanations.

Most of all, I'd like to thank Peter Grütter for his introducing me to this exciting field, for his generous support, for his all too infrequent kicks in the butt, and for his friendship.

Atomic Force Microscopy

Introduction

We live in a tremendously exciting period in the physics world. Almost daily advances in computer simulation techniques are enabling scientists to model larger and larger molecular systems. At the same time, increasingly sensitive microscopes are probing smaller and smaller features of matter. These two advances are set to collide, in the next few years, in a flurry of activity where the theorists and the experimentalists will be able to test their physical models with experiments or vice versa. At the same time, advances in technology are leading us more and more into the realm of the microscopic. The properties and interaction of matter are being tested to new limits daily as moving parts and electronic circuits shrink in size. New tools are surfacing to probe such microstructures.

In the past few years, a generation of microscopes, called Scanning Probe Microscopes (SPM), have risen to become some of the scientist's most powerful tools. These microscopes are able to measure almost every property of a sample surface, including electronic structure, transport properties, and even friction.

An increasingly important member of the SPM family is the Scanning Force Microscope (SFM), also known as the Atomic Force Microscope (AFM) since it is able to measure forces at the molecular, and even atomic, level. The AFM is sensitive to a number of forces, including Coulomb and magnetic forces, making it ideal to investigate conductors, insulator, superconductors, semiconductors, practically any sample surface.

For the past year, the SPM group in the Physics Department at McGill University

has designed and built a general-purpose AFM which we think will be quite successful in experiments on a sub-micrometer scale. The group is lead by Dr. Peter Grütter and includes Yanzhang Liu, Graham Cross, Mark Roseman, Rahma Tabti and myself. This report presents the reader with an introduction to the field of SPM, as well as an overview of the design and important characteristics of the instrument.

INTRODUCTION TO SCANNING FORCE MICROSCOPY

Atomic Force Microscopy has its origins at IBM Zurich where in 1982, Gerd Binning and Heinrich Rohrer developed the Scanning Tunneling Microscope (STM)¹. The microscope measured the tunneling current between the sample and a fine probing tip. The proved to be a very sensitive detector of electronic structure but it lacks the ability to measure interatomic forces. A few years later was born an instrument that could do just that, the Atomic Force Microscope. The principles behind today's generation of AFMs, generically called Scanning Probe Microscopes (SPM) are very similar to the STM and differ, for the most part, only in the interaction between the microscope and the sample surface.

The principle behind Atomic Force Microscopy² is quite simple. Atomic scale forces between a sample surface and a small tip are measured as deflections of a small cantilever to which the tip is attached. A force profile of the sample surface is obtained by raster scanning the tip over the sample. With the use of a sharp enough tip, AFMs may reach atomic, or near-atomic, resolution for some samples. A number of forces between the sample and the cantilever tip may be investigated, including electrostatic, magnetic, van der Waals, and frictional forces. This range of interactions allows us to image many different properties of the sample, including the topography, magnetic structure, friction, adhesion, conductivity and elasticity. Force Microscopes are easily adaptable to various environments, such as a vacuum, low temperatures, and can even be used in a liquid, which enables the imaging of many kinds of samples, including conductors, insulators, superconductors, and even

¹See Binning and Rohrer [82] for the original work on STM.

²See Binning, Quate and Gerber [86] for the original work on AFM.

biological specimens, such as DNA. The versatility of the AFM is ideal for imaging, spectroscopy, and even manipulation on an atomic scale and requires very little or no sample preparation, a tremendous advantage over competing techniques, such as electron microscopy.

The images of the sample surface are obtained by digitizing the deflections of the cantilever, while the sample is scanned, as a function of lateral position. The motion of the cantilever is measured by a sensitive deflection sensor and then analyzed and transferred to a computer for image processing and analysis (see section 3.7). Typical interaction forces between the sample and the tip range from 10^{-12} to 10^{-6} N. This is comparable to the force between two covalently bonded atoms, which is of the order of 10^{-9} N for a separation of about an angstrom (Meyer [92]).

There are two imaging modes: contact and non-contact. While the tip is in contact with the surface, the topography may be mapped out, with great resolution, by dragging the tip across the surface. Also, frictional forces and surface deformations may be investigated in this mode. To measure other, long-range forces, such as magnetic or electrostatic, the tip is lifted out of contact with the surface and hovers 10 to 100 nm above the sample.

In addition to the two imaging modes, there are two operational modes: static, or dc-mode, and dynamic, or ac-mode. In the dc-mode, the interaction force F between the sample and tip will serve to deflect the cantilever. The force on the cantilever beam (CB) is related to the deflection x by a spring constant, k_{CB} , such that $F = k_{CB}x$. The spring constant for a rectangular cantilever is related to the Young's modulus of the cantilever, E, the length l, thickness t, and width w of the lever, by

$$k_{CB} = \frac{Ewt^3}{4l^3}$$

0

H

A cantilever beam of dimensions $1 \times 10 \times 100 \mu \text{m}^3$ made out of silicon ($E = 1.69 \times 10^{11} \text{N/m}^2$) has a spring constant of $k_{CB} = 0.42 \text{N/m}$ which is comparable to a similar sized piece of aluminum foil. Another popular cantilever shape is the triangular, or "V"-shaped, cantilever. These have greater lateral stiffness than the rectangular cantilevers. The "V"-shape corresponds approximately to two rectangular cantilevers

in parallel and the spring constants are coupled accordingly. The resonant frequency of a cantilever is approximated by (Albrecht et al. [90])

$$f_r = 0.026 (E/\rho)^{\frac{1}{2}} \frac{t}{t^2}$$

where ρ is the density of the material used to fabricate the cantilever¹

The dc-mode is used to scan the sample by fixing the cantilever at a constant height above the sample and measuring its deflections as it scans the surface to create a force profile. Alternately, one can fix a constant interaction force between the sample and the cantilever. Here the image is formed from the feedback signal required to maintain the constant interaction force as the sample is scanned.

In the ac-mode, the cantilever is set to oscillate about its resonant frequency. A distance-dependant force F(z) will serve to change the resonance frequency of the cantilever. The ac-mode is sensitive to the force gradients of the tip-sample interaction. As the tip is scanned over the sample surface, the presence of a force gradient $\partial F_z/\partial z$ acts to change the effective spring constant k of the cantilever,

$$k = k_{CB} + \frac{\partial F_z}{\partial z}$$

A repulsive force ($\frac{\partial F_z}{\partial z} < 0$) increases the resonant frequency, $\omega = \sqrt{\frac{k}{m}}$, whereas an attractive force will lower the resonant frequency. By tracking the changes in ω we can determine the changes in the force gradient by (to first order):

$$\Delta F' = \frac{2\Delta\omega}{\omega} k_{CB}$$

With sensitive detection techniques, changes in resonant frequency of below 1 Hz are possible to measure.

As in the dc-mode, there are two ways of controlling the tip in the ac-mode. One can either fix the resonant curve at a certain position during the scan and measure profiles of constant force gradient, or alternately, by disabling the feedback loop, one can acquire variable gradient images. Force gradients in the range of 10^{-5} to 10N/m are obtained. If we assume a simple force law $F(z) = const \cdot z^{-2}$ then we may associate

¹See Chen et al. [94] for a complete look at the resonance response of cantilevers.

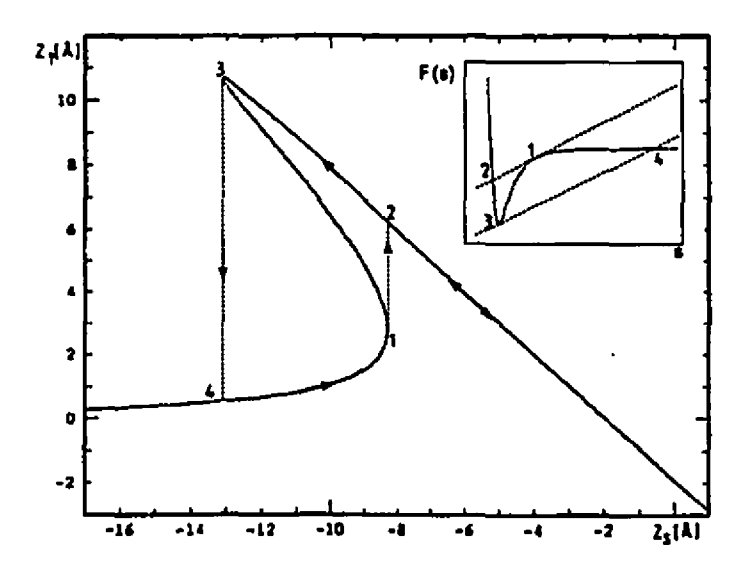


Figure 2.1: Simulated Force vs. Distance plot. Z_t and Z_s correspond to the movement of the cantilever tip and the sample respectively. The tip bends slightly as the sample approaches until the force gradients between them exceeds the cantilever spring constant, at point 1, where the tip snaps to the surface (at point 2). The tip and sample then remain in contact as the sample continues to move against the tip. As the sample retreats, the tip remains in contact until point 3 where another instability occurs. The tip then snaps away from the sample to point 4. The insert shows the corresponding force-distance law, where s is the tip-to-sample distance. From Meyer et al. [88].

the force gradient measurements to actual force measurements in the range (assuming a tip-sample distance of z = 10nm) between 10^{-13} to 10^{-7} N.

Another useful mode of operation is the acquisition of force vs. distance curves (See figure 2.1). In this mode, no lateral motion occurs, but the cantilever and sample are slowly brought together and then apart. The tip deflection (giving the force acting on the cantilever) is monitored as a function of sample position (the distance from tip to sample). An instability typically occurs when the tip is brought close enough to the surface so that the force gradient between the tip and sample is greater than the spring constant of the lever. The tip then snaps to the surface. Similarly, as the tip is pulled away, a point occurs when the restoring force of the lever is stronger than the contact force of the tip on the sample, and the tip springs away from the surface. These curves, and especially the two instability points, are of great interest in many samples.

2.1 Forces

A number of forces are measured using the AFM. Several forces may be investigated on a single sample and during the same scan.

2.1.1 Van der Waals Forces

Although the average charge distribution in a rare gas atom is spherically symmetric, there may be a net dipole moment, p_1 at any instant. An electric field, $E \propto p_1/r^3$ at a distance r from the atom, will induce a dipole moment in another atom $p_2 = \alpha E$ where α is the polarizability of the atom. The dipole will thus have an interaction energy of the order of (Ashcroft and Mermin [76])

$$E \sim rac{lpha p_1^2}{r^6}$$

Since this depends on p_1^2 , its time average does not vanish even if the time average of p_1 is zero. The r^6 dependence means that this force is very weak except at short distances and then especially for atoms whose charge distribution is asymmetric. To complete the picture of interacting dipoles, one must also consider the interacting triplets and higher groupings of atoms, but the effect of these is much smaller than the pair dipoles and falls off much more rapidly.

In AFM, van der Waals (vdW) forces arise from the instantaneous polarization, and following interaction, of atoms in the tip and sample. They are always present in any scan but are usually small (< 1 % as large, depending on the size and shape of the tip) compared with electrostatic or magnetic forces. Only when then tip-to-sample distance decreases to about 1nm do the vdW forces start to dominate the interaction with forces in the nanonewton range.

2.1.2 Electrostatic Forces

The exact mechanism for charge transfer at insulator-insulator, insulator-metal and metal-metal interfaces is not well understood and is crucial in many scientific and

industrial applications. These include the tribocharging of water molecules and ice particles which lead to lightning, the charge transfer in electric switches, as well as the critically important motion of charges in semiconductors.

The force on a conductive tip due to a charge distribution on an insulating sample is given by

$$F_{charge} = q_{tip}E_z$$

where q_{tip} is the induced charge on the tip and E_x is the electric field due to the charge distribution. A voltage V is often applied to the sample to control the charge level and so the charge on the tip has two components $q_{tip} = -(q_{surface} + C \cdot V)$ where $q_{surface}$ is the charge induced on the tip by the sample charge distribution and $C \cdot V$ is the charge applied externally across the tip-sample separation of capacitance C. This capacitance contributes to the total force by

$$F_{capacitance} = rac{1}{2} rac{\partial (CV^2)}{\partial z} = rac{V^2C'}{2}$$

The total force is then

$$F_{total} = F_{charge} + F_{capacitance} = -(q_{surface} + C \cdot V)E + \frac{V^2C'}{2}$$
 (2.1)

To first order, E_z is proportional to the charge on the sample (for small tip-sample separations, $E_z \propto \sigma$ the surface charge density), the first two terms are a measure of the charge distribution on the sample. The sample voltage is used to modify the total force in order to differentiate the electrostatic signal from other forces, such as van der Waals forces. In fact, if the voltage is modulated sinusoidally $V = V_0 + V_1 \cos(\omega t)$, the capacitive signal may be measured as an ac signal of frequency 2ω whereas the charge contribution is measured as a dc signal and a signal at frequency ω .

A spherical tip of radius R will experience a capacitive force of roughly (Meyer [92])

$$F_{capacitance} = \frac{-\pi \epsilon_0 RV^2}{z_{effective}}$$

 $^{^{1}}E_{s}$ and E_{y} serve to twist the cantilever instead of deflecting it. They are not present for conductive samples since the charges are free to move.

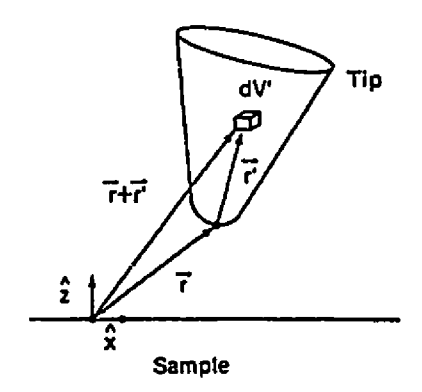


Figure 2.2: Coordinate system used in determination of magnetic forces. From Rugar et al. [90].

at an effective distance $z_{effective} = z + h/\epsilon$ above the surface of a sample of thickness h and dielectric constant ϵ . Being independent of charge, $F_{capacitive}$ can be used to measure the local dielectric constant or, alternatively, the radius of the tip. This analysis is often done in Magnetic Force Microscopy (MFM).

2.1.3 Magnetic Forces

There is tremendous excitement in both the scientific and industrial communities at the ability to measure small magnetic domains using force microscopy techniques. Much hope exists that this technology will lead to breakthroughs in data storage devices, as well as a deeper understanding of magnetics on a molecular level. The stray field from the sample, $\mathbf{H}(\mathbf{r})$, can be calculated from the sample magnetization, \mathbf{M}^{S} , according to¹

$$\begin{split} \mathbf{H}(\mathbf{r}) &= -\int_{sample\ volume} \nabla \cdot \mathbf{M}^S(\mathbf{r}'') \ \frac{\mathbf{R}}{|\mathbf{R}|^3} \ dV'' \\ &+ \int_{sample\ volume} \hat{\mathbf{n}}_S \cdot \mathbf{M}^S(\mathbf{r}'') \ \frac{\mathbf{R}}{|\mathbf{R}|^3} \ dV'' \end{split}$$

where $\mathbf{R} = \mathbf{r} - \mathbf{r}''$, $\hat{\mathbf{n}}_S$ is the outward unit normal from the sample surface, $\nabla \cdot \mathbf{M}^S$ is the volume magnetic charge and $\hat{\mathbf{n}}_S \cdot \mathbf{M}^S$ is the surface magnetic charge density. Once the stray field from the sample is known, we can calculate the force and force

¹See Grütter and Allenspach [94], or Güntherodt and Wiesendanger [92], for a more complete discussion of MFM.

2.1 Forces _______ 11

derivative acting on the tip. The force acting on a volume element in the tip is

$$d\mathbf{F}_{mag} = \nabla_{\mathbf{r}} [\mathbf{M}^{T}(\mathbf{r}') \cdot \mathbf{H}(\mathbf{r} + \mathbf{r}')] dV'$$
 (2.2)

where $M^{T}(\mathbf{r}')$ is the magnetization of the volume element in the tip. The force derivative is

$$dF'_{mag} = \hat{\mathbf{n}} \cdot \nabla_{\mathbf{r}} (\hat{\mathbf{n}} \cdot d\mathbf{F}_{mag}) \tag{2.3}$$

A number of approximations are used to simplify this general picture. First, it is assumed that the magnetization of the tip and that of the sample don't affect each other, that is, that \mathbf{M}^S and \mathbf{M}^T are constant. Also, we assume that the cantilever is parallel to the surface, that is $\hat{\mathbf{n}} = \hat{\mathbf{z}}$. Then, we may simplify 2.3 to

$$dF'_{mag} = \frac{\partial^2 \mathbf{F}_{mag}}{\partial z^2}$$

A difficulty arises here in that it is not possible to uniquely determine the sample magnetization from a measurement of the stray field (Grütter and Allenspach [94]). This is because for every given magnetization, it is possible to add a magnetization component, where $\nabla \cdot \mathbf{M}^S = 0$, which does not alter the stray field. To proceed, one first assumes a sample magnetization and calculate the stray field. Second, one then assumes a tip magnetization and integrates to find the magnetic force. We can then compare the theoretical prediction to the experimental result. The final step is to start back at the beginning and test the various parameters to check self-consistency and to try and refine the model used in the calculations.

There are two simplified cases. First, we may assume that the tip consists of a point dipole m, so that

$$F_{may} = m_x \frac{\partial H_x}{\partial z} + m_y \frac{\partial H_y}{\partial z} + m_z \frac{\partial H_z}{\partial z}$$

$$F'_{mag} = m_x \frac{\partial^2 H_x}{\partial z^2} + m_y \frac{\partial^2 H_y}{\partial z^2} + m_z \frac{\partial^2 H_z}{\partial z^2}$$

In this case, if we scan a sample while keeping the force constant, we probe the derivative of the stray field and while keeping a constant force gradient, we measure the second derivative.

For our second simplified case, we may consider a very long tip domain in which case only one pole interacts with the surface and so

$$F_{mag} = \mathbf{M}H_z$$

$$F'_{mag} = \mathbf{M} \frac{\partial H_z}{\partial z}$$

where M is the dipole moment per unit length. In this case, the stray field itself is investigated during a constant force scan while the first derivative is probed using the constant gradient mode. For many tip geometries, the monopole tip approximation more accurately describes the experimental results (Schönenberger and Alvarado [90]).

One must be careful with the tip-sample interaction as samples made of magnetically very soft materials may be difficult to image correctly since the stray field from the tip may influence, or even reverse, the magnetization of the sample (see Güntherodt and Wiesendanger [92], volume II, chapter 5).

2.1.4 Other Forces

Capillary Forces

Force measurements performed under ambient conditions are influenced by the interaction of vapors with the sample surface. This usually takes the form of a thin film, usually water, covering the surface of the sample. The force of interaction between the film's meniscus, of area A, and the probing tip, of radius R is (Meyer [92])

$$F_{capilary} = rac{\gamma 2\pi Rd}{r_1 + r_2}$$

where γ is the surface tension, d is the tip penetration depth and r_1 and r_2 are the meniscus radii. For a typical cantilever tip, the capillary forces are of the order 10^{-7} N which is about 10 times the van der Waals contribution between the tip and sample surface. This force can be used to characterize the sample but often interferes with

the scan instead.

Ionic Repulsion Forces

While the tip and sample are in contact, Coulomb repulsion between the nuclei in the sample and in the tip, as well as Pauli's Exclusion Principle prevent further penetration of the tip into the sample. These forces are very strong and very short ranged, decaying away within tenths of angstroms. These forces overshadow the other, long-ranged, forces during contact and are the principle forces behind contact mode microscopy as described above.

One usually uses one of three potentials to describe the contact forces¹. The first is a hard sphere potential

$$U(r) = \left\{ egin{array}{ll} 0 & ext{for } r \geq r_0 \ \infty & ext{for } r < r_0 \end{array}
ight.$$

where r_0 is the hard sphere diameter. The second potential is a power law of the form

$$U(r) = \left(\frac{\mathrm{const}}{r}\right)^n$$

where n is usually 12. The final potential is an exponential

$$U(r) = (\mathrm{const})e^{-r/r_0}$$

where $r_0 \simeq 0.2$ Å. The exact form is of little practical importance save that it is short-ranged.

The vdW forces are not negligible in contact mode if there is much interaction between many atoms in the tip and the sample. This occurs if, for example, the tip is rather broad (Hutter and Bechhoefer [93]). It is possible to reduce the vdW forces by either having a sharp tip, or by immersing the tip and sample in a liquid medium for which the vdW interactions between the tip and sample will be weak and repulsive (Hartmann [91] and also Drexler [91]).

¹See Israelachvili [91] for an in-depth look at atomic potentials.

Frictional Forces

With the tip in contact with the surface, it is possible to measure the frictional forces on the sample surface. This is usually done by dragging the cantilever tip sideways across the sample and measuring the lateral twisting of the cantilever by laser beam deflection methods (see next section). In many ways, the use of a force microscope to image friction is ideal. The small tip makes for a contact area between the tip and sample that is equal to the real contact area that is, a single asperity (the large, rough interface between macroscopic samples is difficult to account for in theoretical models). The small contact area (in the order of nm²) between the tip and sample allows the investigation of the cause and effect of friction on a near-atomic level. By adjusting the position of the cantilever, one can easily modify the load pressure (in the range of GigaPascales) to control the wear and plastic deformation of the surface.

2.2 Force Sensors

The combination of a sharp tip and a flexible cantilever is the most important part of any SPM. By varying the parameters of size, composition, and coating, a number of different force sensors may be constructed.

The two most critical components of the cantilever are the spring constant and the tip. A small spring constant will make for a sensitive lever, but these are more susceptible to crashing into the sample when tip-to-sample force gradients exceed the spring constant. The size and shape of the tip will determine the force the cantilever is exposed to at a distance away from the sample. The cantilever beam may be constructed out of a host of different materials using a number of techniques in a variety of shapes and sizes. Cantilevers made of etched wires and foils were popular until microfabricated ones became available. In our system, we will primarily be using microfabricated silicon and silicon nitride cantilevers, both with integrated tips. The microfabricated tips are primarily pyramidal in shape but tips may be sharpened into a conical form, with high aspect ratios, by anisotropic etching (see Farooquit

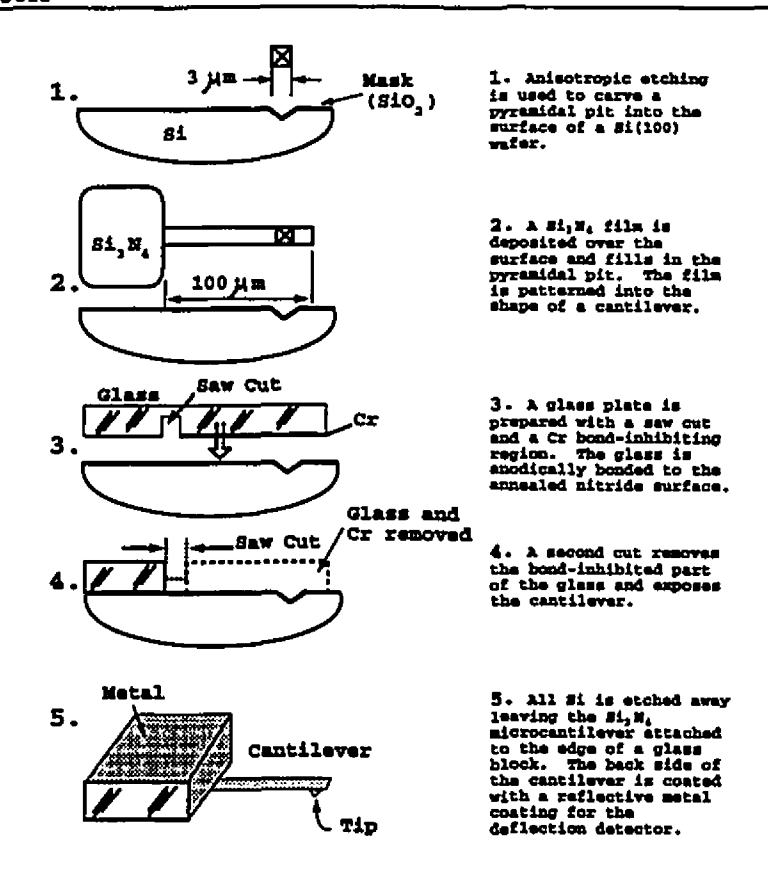


Figure 2.3: Microfabrication of silicon nitride cantilevers with integrated pyramidal tips. Adapted from Albrecht et al. [90].

et al. [92]). The tips can be functionalized by various coatings, and so be sensitive to specific interactions. For example, a tip coated with cobalt is sensitive to magnetic forces. The process used to microfabricate cantilevers is similar to that of assembling integrated circuits (see figure 2.3 for a popular microfabrication technique for Si₃N₄ cantilevers). See Albrecht et al. [90] for a review of cantilever microfabrication and Tortonese et al. [91] for a look at AFM using piezoresistive cantilevers.

The mechanical characteristics of the cantilever depend on the material it is made of as well as the size and shape of the lever. Typical dimensions for our rectangular Si_3N_4 cantilevers are $1 \times 20 \times 200 \mu m^3$ with a spring constant of 0.02 N/m, a resonant frequency of 15 kHz and a Q-factor of 20 in air (550 in high vacuum of 10^{-8} Pa). The single crystal silicon cantilevers we are using for MFM have a spring constant of between 1.8 and 5 N/m, a resonant frequency of about 84 kHz, and a Q-factor of 200 in air (40000 in high vacuum). Of course, cantilevers exist within a large range

of characteristics.

The cantilever tip is also very important for sensitive measurements. The tip characteristics of height, radius and cone angle are necessary for correctly interpreting AFM images. An ideal tip would end in a single atom, but this is unlikely to occur because of oxidation of the tip and the presence of adsorbed atoms. It is reasonable, though, to expect a radius of only a few nm for microfabricated cantilevers. Since most applications of SFM probe only the relative strength of the forces on the surface, a perfectly sharp tip is not necessary.

2.3 Deflection Sensors

A number of different sensors may be used to measure the deflections of the cantilever. The original device measured the tunneling current between the back of the cantilever and a sharp tip. This proved effective (cantilever deflections of 10^{-2} Å are resolvable) but difficult to implement since the tunneling is critically affected by contaminants and poor signal-to-noise ratios are usually achieved since the probe-to-tip tunneling is often comparable to the surface-to-tip tunneling.

The two most used methods rely on laser light reflected off a metallic coating on the back of the cantilever. One can either deflect the light onto a sensitive photodetector¹ (see figure 2.4) or use an optical fiber to bring the laser light to within microns of the back of the cantilever (see section 3.3). Most of the commercial instruments use the beam deflection method whereas most custom built microscopes (including ours) rely on the interferometry method². Both systems can typically measure beam deflections

¹The photodetector is partitioned into either 2 sections, one above the other, or 4 sections arranged in a square. The difference in signal between the top and bottom halves determines the vertical deflection of the cantilever. The difference in signal between the right and left halves gives the lateral twisting of the cantilever which is usually attributed to friction. See Sarid [94] for the performance of the deflection system.

²Rahma Tabti is currently designing a beam deflection adapter for our microscope based on work by Matthew Pelton. In addition, we have received a set of piezoresistive cantilevers. This will allow us to, among other experiments, compare three deflection methods on the same experimental setup.

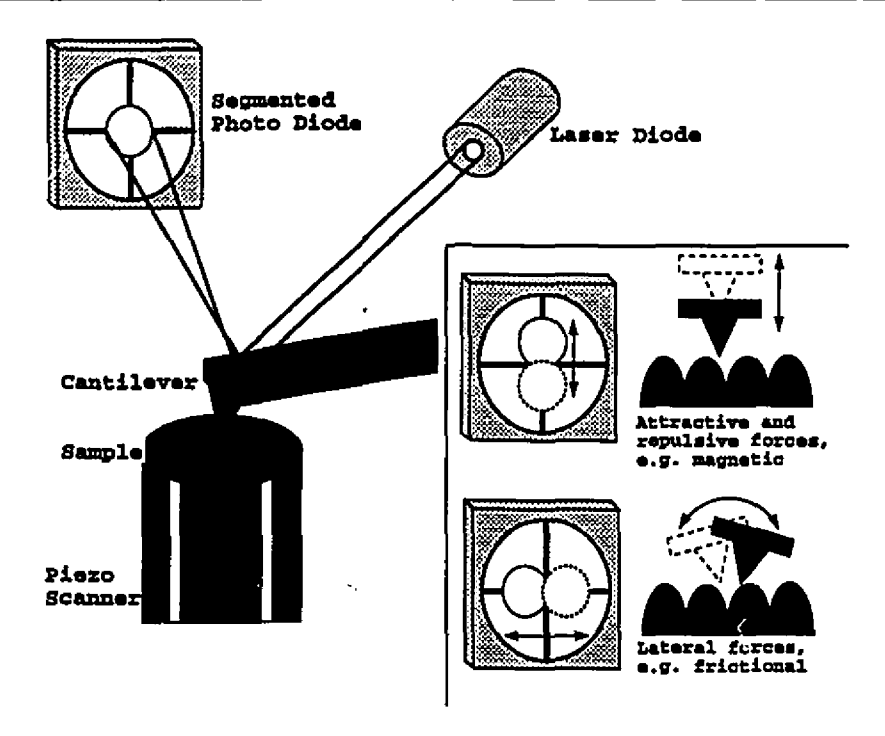


Figure 2.4: Schematic of beam deflection setup. A laser beam is reflected off of the tip of the cantilever into a four-quadrant photodetector. Vertical and twisting motions of the cantilever are measured as vertical and horizontal shifts, respectively, of the laser beam position. Adapted from figure 1.39 of Marti [93].

of $10^{-4} \text{\AA}/\sqrt{\text{Hz}}$.

A new class of cantilevers using piezoresistance elements has recently generated much excitement. The promise is that the cantilever can now be used as both the force sensor and the deflection sensor. This eliminates the need for external deflection sensors which are often difficult to position and awkward to include in some experiments. The deflection of the cantilever changes the resistance of a tiny circuit microfabricated onto the cantilever. Once calibrated, this resistance change allows Angstrom precision measurement of the cantilever deflections. See Tortonese et al. [91] for more details on piezoresistive cantilevers.

The last popular method of detecting cantilever motion is the capacitance method. A small electrode is placed near the back of the cantilever which measures the capacitance signal across to the back of the cantilever. The signal is very sensitive to the electrode-cantilever distance and deflections of 0.1 Å are detectable.

See Fujisawa et al. [94] for a preliminary work on the comparison of both optical methods.

2.3.1 Interferometry

In this detection method, a laser beam is split into a reference beam (of intensity I_0) and a beam which reflects off of the cantilever (of intensity I_r). The two beams then recombine and the superposition has an intensity I given by

$$I = I_0 + I_r + \sqrt{I_0 I_r} \cos(\Phi)$$

where Φ is the phase difference between the electric fields of the two beams which depends on the optical path length difference between the two beams:

$$\Phi = \Phi_0 + \frac{4\pi\Delta z}{\lambda}$$

where Δz is the deflection of the cantilever and λ is the wavelength of the laser. To increase the sensitivity, the position of the cantilever is adjusted so that the phase difference is shifted to $\Phi_0 = m\pi/2$, where m is an integer, to make the relative variations of the intensity

$$\frac{\Delta I}{I} = \frac{2\sqrt{I_o I_r} \frac{4\pi \Delta z}{\lambda}}{I_o + I_r} \tag{2.4}$$

which, for $I_o \simeq I_r$, reduces to

$$\frac{\Delta I}{I} = \frac{4\pi\Delta z}{\lambda} \approx \frac{\Delta z}{\lambda} \tag{2.5}$$

The spectral sensitivity is limited by the shot noise of the photodetector which generates a current of $I_{shot} = \sqrt{2eIB}$ where e is the electronic charge, I is the current of the photodetector output and B is the bandwidth. For frequencies below a few kHz, other noise sources, especially 1/f noise, limit the sensitivity. See the appendix for a discussion of electronic noise sources.

For a stable system with low-noise electronics, the relative variations can be measured to $10^{-4}\text{\AA}/\sqrt{\text{Hz}}$ at frequencies above a few 100 Hz. This is the noise limit given by photon statistics (the interferometer is limited by the discreteness of the incident light quanta). The sensitivity of a properly designed SFM should be limited by thermal vibrations of the cantilever (Albrecht et al. [91])

$$F_{min_{thermal}} = \sqrt{\frac{4k_B k_{CB} TB}{\omega Q}} \tag{2.6}$$

$$F'_{min_{thermal}} = \frac{1}{A} F_{min_{thermal}} \tag{2.7}$$

where k_B is the Boltzmann constant and Q is the quality factor of the cantilever, and A is the rms amplitude of the lever oscillations (~ 10 nm). The thermal vibrations are typically around 10^{-11} meters in amplitude. The 1/A factor in the force gradient sensitivity allows increased sensitivity when the tip is far away from the sample.

2.4 Piezoelectrics and their Associated Nonlinearities

A special class of materials, called piezoelectrics plays a crucial role in AFM. The crystal structure of piezoelectrics has an inherent polarization so that in an electric field, a strain is present on the lattice. Conversely, if the crystal is strained, an electric field develops. The effect is akin to magnetism with crystal polarization taking the place of magnetic moment. In AFM, both the sample and the cantilever are often controlled to atomic precision by piezoelectric actuators. By applying a suitable electric field across the piezoceramic, we are able to sensitively control the motion of the cantilever and the sample.

The piezoelectric scanner responds linearly with applied voltage, to first approximation. The ideal relationship between the strain and an applied electric field is

$$s = dE$$

where s is the strain in Å/m, E is the electric field in V/m and d is the strain coefficient in Å/V. The strain coefficient is characteristic of a given piezoelectric material, usually some form of lead zirconium titanate (PZT) in piezos used in SFM, and has a value of 10-100 Å/V. There are a number of methods of calibrating the piezoelectric material used in AFM. In our microscope, the sample is fixed to a piezoelectric tube scanner (see section 3.2) which was calibrated using two different methods. The sensitivity in the x and y directions was determined by scanning a grating with grooves spaced $1.6 \mu m$ apart. By counting the number of grooves in the scanned image, one similar to figure 2.5, we can calibrate the motion of the scanner in one lateral direction. We then rotate the sample, or use a 2 dimensional grid instead, to measure the other



Figure 2.5: Image of a 1.6 μ m grating. The lateral sensitivity of the piezoelectric scanner is calibrated by comparing the voltage applied to the piezo to the actual displacement. Hysteresis and creep of the piezo may be seen on the image as a slight curbing of the grid lines which are actually straight. The curbing is most prominent at the edges of the scan. The image courtesy of Yangshang Liu.

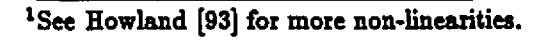
lateral sensitivity. The z direction was calibrated by using the laser interferometer (see section 3.3). The laser beam is shone directly onto a reflecting sample which is raised and lowered on the piezoelectric scanner. Each time the interferometer goes through a fringe, the sample height has change by $\lambda/4$ and so the piezo sensitivity may be calibrated in the vertical direction.

In practice, the behavior of piezoelectrics is not perfectly linear. A number of divergences arise that are intrinsic to the material. A brief description follows¹.

2.4.1 Hysteresis

In addition to the intrinsic nonlinearities, the piezoelectric ceramic also displays hysteretic behavior. The extension of the scanner differs depending on whether it is extending of contracting (see figure 2.6).

The hysteretic effect is due to the fact that as you increase the electric field, or the strain, it becomes more and more difficult to change the orientation because of the growing number of aligned domains working against you. This may account for a divergence of up to 20% in some cases.



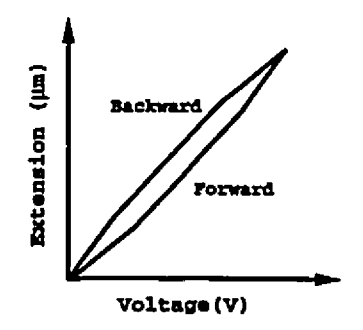


Figure 2.6: Hysteresis in piesoelectrics. Since extension takes more voltage than contraction, the surface will appear lower after a step on the sample. To minimize the effect of hysteresis, data is usually taken in only one fast-scan direction, though interesting effects may be observed by comparing both directions. Adapted from Howland [93].

2.4.2 Creep

When an abrupt change in voltage is applied, the piezoelectric material does not change all at once. Instead, the dimension change occurs in two steps: one change occurs quickly (< 1 millisecond) and extends the scanner most of the way. The second step takes much longer (< 100 seconds) and is known as creep (see figure 2.7). The creep is caused by the fact that once you reorient a series of domains, the new orientation will induce some of the neighboring domains to follow. The gradual increase in the oriented domains increases the strain on the piezo which will tend to bend slightly further.

Because of creep, it becomes more difficult to "zoom in" to a region of the sample. By applying an offset voltage to the scanner, one can focus in to a particular section of the sample, but the offset must be updated or the creep will cause you to miss the region of interest as the scanner drifts (creeps) out of the area. Thus one must wait for the creep to pass before imaging. Comparing successive scans will help determine the amount of creep left. It is possible to correct for hysteresis and creep by suitable data algorithm (see Jorgensen, Carneiro and Madsen [93]) or by accurately determining the actual position of the scanner by the use of lasers, capacitor, etc (see Barrett and Quate [91]).

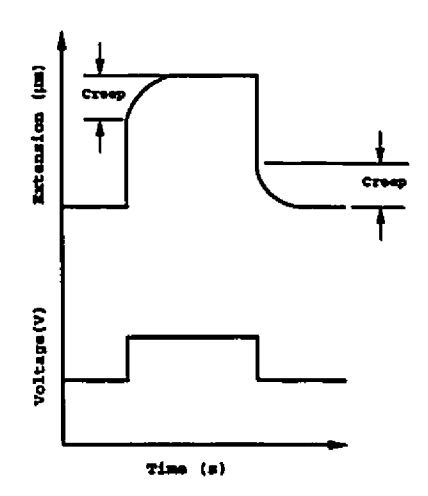


Figure 2.7: Piezo creep will result in that scans taken at different scan speeds will show slightly different length scales (magnifications). The effect in the vertical (z) direction is even more noticeable. As the cantilever tip traverses a step, the scanner contracts immediately with a voltage corresponding to the full step height. During the next few seconds, the scanner will continue to contract slowly as creep occurs. To keep the tip at the same height, the SPM must apply a voltage in the other direction, counteracting the creep. The same thing will happen when the tip encounters a dip instead of a step. The result is that creep will cause ridges to appear on one side a a feature and trenches on the other side. Comparing both fast-scan direction images will help separate creep artifacts from true features. Adapted from Howland [93].

2.4.3 Cross Coupling

Cross coupling refers to the tendency of x-axis or y-axis scanner movement to generate a spurious z-axis component. There are several sources: the fact that the electric field is not constant across the scanner, that the strain fields are not simple constants but actually complex tensors, and that there exists some "cross talk" between the x, y, z electrodes. The cross coupling will cause a SPM to generate a bowl-shaped image of a flat sample.

The most important contribution is geometric. The sideways motion of the scanner is produced when one side of the tube shrinks, and the other expands. The results is a piezo tube that scans in an arc, not in a plane. Also, a thicker sample will trace out a larger arc than a thin one. For our microscope, these effects are small. Our 2 inch long piezo scanner is such that if one sample differs from another by 1 mm, the scans of the two will be similar, with only a 0.07% difference in the lateral scale.

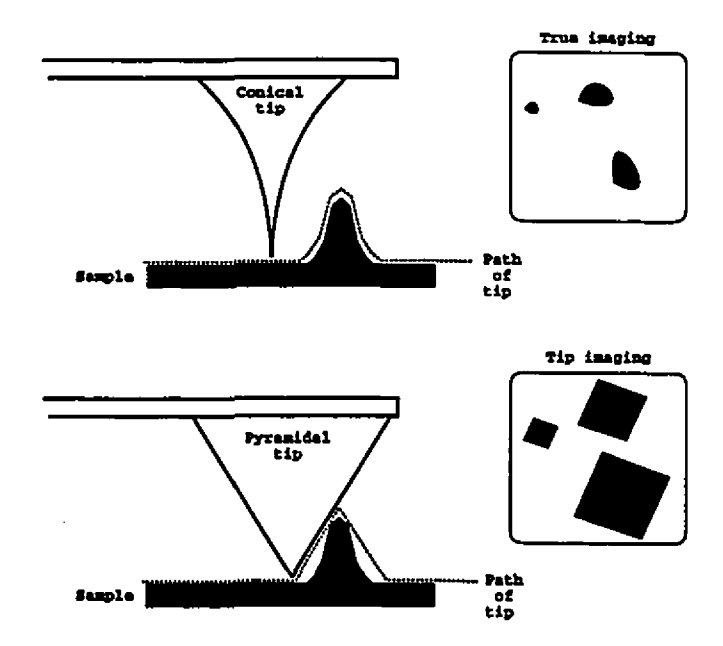


Figure 2.8: Tip convolution effect. A sharp conical tip takes the true image of the structure. A large, pyramidal tip generates an artifact which depends on its size. Adapted from Howland [93].

2.5 Other Artifacts

Many artifacts in SPM are attributed to tip imaging. Each point on an SPM image represents a spatial convolution of the shape of the tip and the shape of the structure imaged. A true image of the feature is possible as long as the tip is much sharper than the feature itself. Unless this is the case, the image will be dominated by the shape of the tip (see figure 2.8.)

The SPM tip is sensitive to a number of different forces. This gives the microscope its versatility but artifacts may be present in an image when the tip picks up a force other than the one you want to focus on.

The feedback electronics may introduce artifacts if not properly optimized. Too high a gain can cause the system to oscillate, creating high frequency periodic noise. Too low a gain can cause images to loose detail. Also, "ghosting" may occur on steep slopes where the tip overshoots as it travels up the slope and again as it comes back down. The result is an image with bright ridges on the uphill side and dark shadows on the downhill side of the feature.

Image processing is an integral part of the microscope. The software can enhance curvature, magnify scale, filter bad data and a number of other operations necessary to properly understand the image features. Used carelessly, though, the data processing can create its own artifacts. For example, random noise may be amplified and filtered to appear like a close packed layer of atoms.

2.6 All is not lost

It may seem, according to the artifacts and non-linearities above, that there is little hope of actually properly imaging a surface. Actually, the prospects aren't nearly as bleak as they seem. An experienced microscope user can quickly differentiate the true image from the artifacts and make the adjustments necessary to eliminate them.

Some steps you can take to test whether your image is true are:

- Repeat the scan to detect creep.
- Change the scan direction and rotate the sample to detect tip imaging
- Change the scan size to detect scaling artifacts
- Change the scan speed or feedback gain to detect feedback artifacts

This is the end of the introduction. There are many review papers, as well as a series of books, that provide a more complete review of the field of AFM. An especially good source is Güntherodt and Wiesendanger [92].

MICROSCOPE DESIGN AND CHARACTERISTICS

My involvement with the SPM group at McGill has been in the familiarization with the field and in the building of our first microscope. I was primarily involved in the construction of the vibration damping stage for the microscope, the building of an electromagnet to be used in magnetic force microscopy, and the setup of our data acquisition and image analysis networks. Please see figure 3.1 for a picture of our microscope and figure 3.2 for the basic operation components of the microscope. The microscope is designed to operate in a high vacuum at room temperature. There are two major challenges in designing an AFM. One is that the force sensor and sample must be accurately positioned and finely controlled down to atomic dimensions. To accomplish this, both coarse and fine adjustment controls are used. The coarse adjustments control the position of the components down to a few micrometers, the fine positioning controls to the last few nanometers or even smaller. The other challenge is the isolation of the microscope against external vibrations. Since the deflection sensor measures changes in amplitude of the cantilever that are orders of magnitude smaller than the large vibrations produced by external sources, such as the building vibrations, the microscope must be properly shielded from vibrations.

The most important parts of the microscope are described below.

3.1 General Design

The microscope is separated into two major parts: the microscope head, which controls the cantilever and deflection sensor, and the support plates, which isolate the

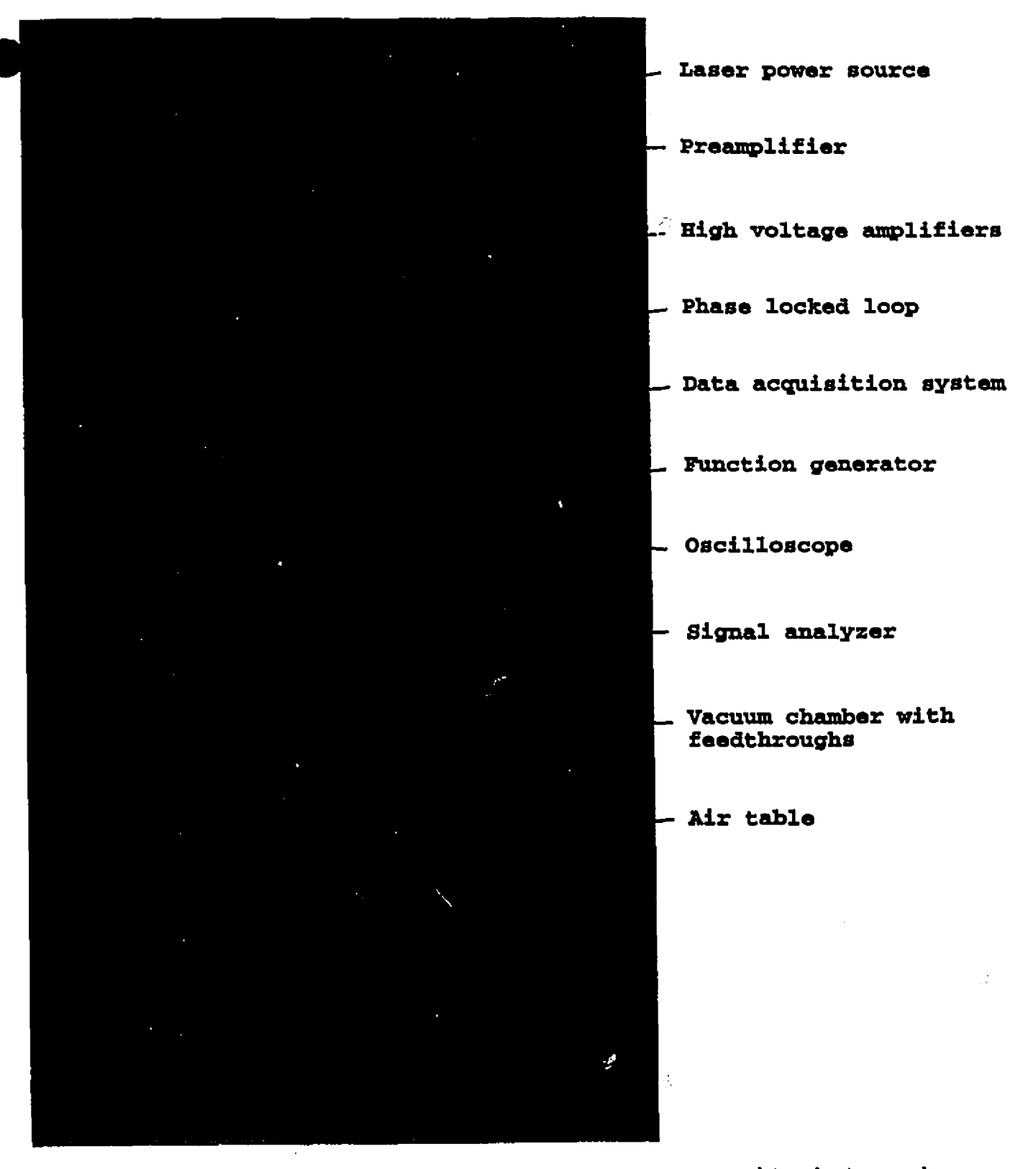


Figure 3.1: Overview of the complete microscope. Many components must work together to properly image a surface.

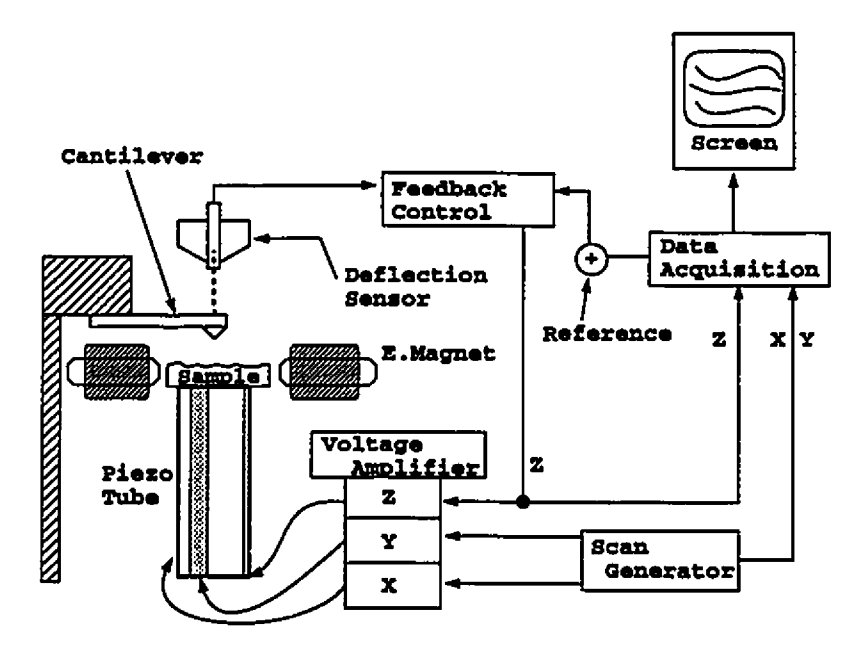


Figure 3.2: The basic operating components of the microscope. Cantilever deflections are detected by a deflection sensor which are analyzed by a feedback control and sent to form an image on a screen. The feedback also controls the vertical position of the sample below the cantilever. The sample is moved by a piezoelectric tube. The electromagnet is placed as near as possible to the sample to provide the greatest magnetic field.

cantilever from vibrations and control the sample and the sample scanner. The stainless steel microscope head (see figure 3.4) has both coarse and fine adjust elements. A number of these elements control the cantilever and position the fiber above the tip. The cantilever itself, as it is assembled, is attached to a comparatively large piece of glass or metal. We silver paint the cantilever onto a piezoelectric bimorph used to control the vertical position of the cantilever above the sample surface. The bimorph is glued to a square piece of glass which electrically insulates the bimorph and cantilever from the rest of the microscope head. The glass square is glued to the end of a 2cm long, 1 mm thick piece of aluminum which is fitted into a narrow slot on the head and held there by two screws (see figure 3.3). The cantilever may be tilted by up to 150, by tilting the aluminum piece, in order to adjust the angle of the cantilever above the sample. This is to allow the tip to scan freely over the surface without having the long cantilever portion of the sensor crashing into surface features. A micrometer screw is positioned so that the end of the threaded section, which ends in a ball bearing, rests on the aluminum. This screw is adjusted to coarsely position the cantilever near the end of the optical fiber. This layering of components allows

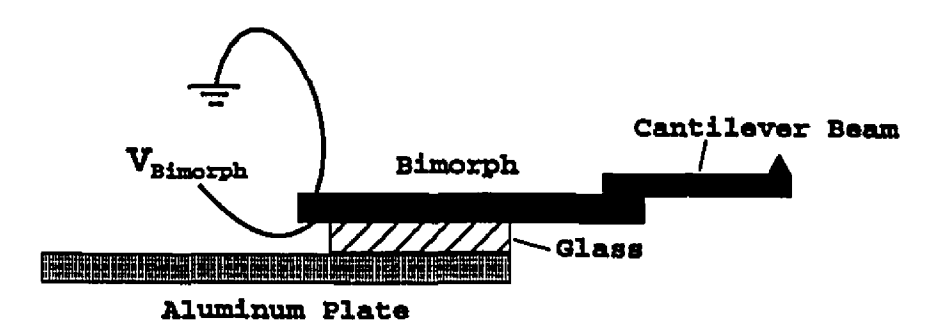


Figure 3.3: The cantilever is attached to the microscope head by first being silver painted onto a piezoelectric bimorph. The bimorph controls the vertical fine positioning of the cantilever above the sample surface. The bimorph is glued onto a square of glass to insulate it electrically from the rest of the head. The glass is glued to a piece of aluminum which is then held in place in a slot in the head by two screws.

for rough positioning of the cantilever (done by the micrometer screw) and fine positioning (done by the bimorph). The last centimeter of optical fiber is glued into a fiber chuck which is coarsely placed into position through a slot in the microscope head, then held in place using a set screw. The fiber chuck can be maneuvered in the horizontal plane by four screws so that fine adjustments can be made. The position of the laser beam above the cantilever tip is fine and critical so we optimize this using an oscilloscope to measure the signal reflected off the cantilever onto the photodetector¹. The final optimization of the fiber above the cantilever takes quite some practice and, in my experience, quite a few errors but the learning process goes on. See figure 3.5 for a 100× magnification of the optical fiber positioned above the cantilever.

The microscope head is supported by three Newport micrometer screws (0.30 mm/turn) and secured in position over the sample by three strong springs. The micrometer screws act to level the head and to roughly position the cantilever, attached to the head, over the sample which is attached to the scanner which is attached to the top damping plate (see figure 3.4). The micrometer screws end in a ball bearing. A conical hole was made into the microscope head for one ball bearing. The second screw's bearing lies in a triangular grove that runs for 10 mm on the opposite side of the microscope head. The third bearing rests on a flat surface to form an isosceles triangle with the two others. This positioning, known as a kinematic mount, uniquely defines an orientation for the head by constraining the six degrees of freedom. The

¹See section 3.3 for a look at our laser optics.

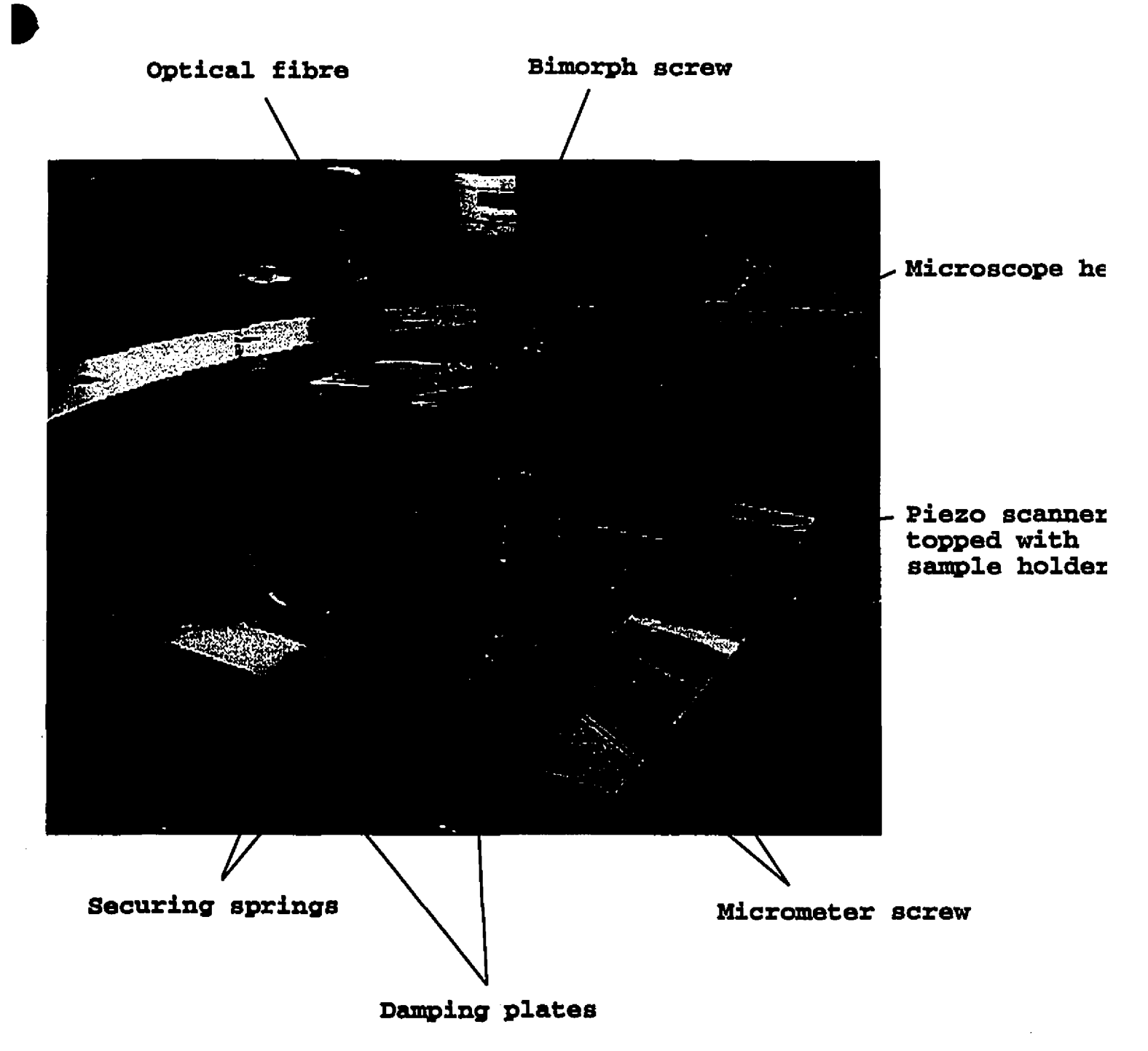


Figure 3.4: A view inside the microscope. The sample rests on top of a piesoscanner which itself is fixed to the top vibration damping plate. The cantilever is fixed to the microscope head which rests on three micrometer screws and is secured by three springs.



Figure 3.5: The positioning of the optical fiber above the cantilever tip. This image, taken by a video camera through an optical microscope, gives an idea of the small scales involved. The image is magnified 100 times—you can barely see the cantilever at all when looking at it with just your eyes.

microscope head is held in place by three springs. The springs are fixed to the top damping plate and are threaded through three holes in the microscope head, then they are pulled taught and a steel pin is inserted across the hole diameter to hold the springs in place. This provides excellent stability and rigidity.

The two screws located nearest the cantilever are adjusted manually by two 2 1/2" gears screwed onto the base plate. These serve to roughly position the cantilever. The other screw is controlled by a small dc motor made by Micro Mo (series 1101-00G) uses a 1024:1 reduction gear (series 1016) to make fine adjustments to the screw and ensures that the screw will actually turn even with the weight of the head on top of it. The position of the third screw away from the cantilever produces a mechanical reduction of the respective tip-sample motion by a factor of 5. This allows very fine adjustment of the cantilever height. The fine positioning of the cantilever over the sample is done by the piezoelectric sample holder itself.

The 1/4" thick stainless steel base plate serves to anchor the microscope and rests at the bottom of the vacuum chamber. The motor and the gears used to control the

micrometer screws are fixed to the base plate by a small brace, in the case of the motor, and by screwing down the gears¹.

There are twelve tapped holes around the edges of the base plate that may be used to secure various devices, such as an electromagnet, used in the microscope.

3.2 Sample Scanner

A flexible tube topped with a sample holder and connected to a scan generator makes up our sample scanner. The tube is made of piezoelectric material. Once calibrated, the bending is very sensitive to changes in voltage and quite reproducible. Please see section 2.4 for more on piezoelectrics. Our longest scanner tube is two inches long and has a scan range of $35\mu m$ in the x and y directions and $2.5\mu m$ in the z direction. Tall tubes have a greater scan range but smaller tubes have greater precision². The outer piezo electrode is split into 4 segments to provide lateral +/-x and y motion. The displacement sensitivity in the x and y directions is 400 Å/Volt. The z sensitivity is 25 Å/Volt. The sample holder consists of two parts (see figure 3.7). The first part is a small cylinder glued to the top of the scanner tube. A pin hole is drilled in the cylinder and a set screw is positioned perpendicular to the hole. The second element is a thin aluminum disk with a guide pin underneath which is inserted in the cylinder and held in place with the set screw. A sample of interest is glued onto the

¹So that the gears would not unscrew when turned, the tightening screws are held in place with a nut dipped in Lock-TiteTM, a cylindrical bonding glue. The nut must be tightened just enough so that the screw assembly rotates freely but is still securely held in place. A difficulty arises since the glue expands when it dries and so the screw will be more tightly fixed around the nut. It took quite a few tries to get the right level of tightness. I finally settled on screwing the nut moderately tight around the screw then loosening it one full turn. Also, it is best not to heat the glue, to get it to dry faster, since it will cose out of the nut and the bond will be weak.

The scanner tube is controlled by three Ergonomics AG high voltage amplifiers, one to move it in each of the x,y, and z dimensions. A voltage step will cause the tube to bend in one dimension. The angle the tube bends to is independent of the length of the tube, but the arc subtended depends on the length of the tube. Thus a smaller tube will be able to move in smaller increments than the large tube. Also, some nonlinearities in the behavior of the piezoelectric (see section 2.4) increase with the size of the piezoceramic.

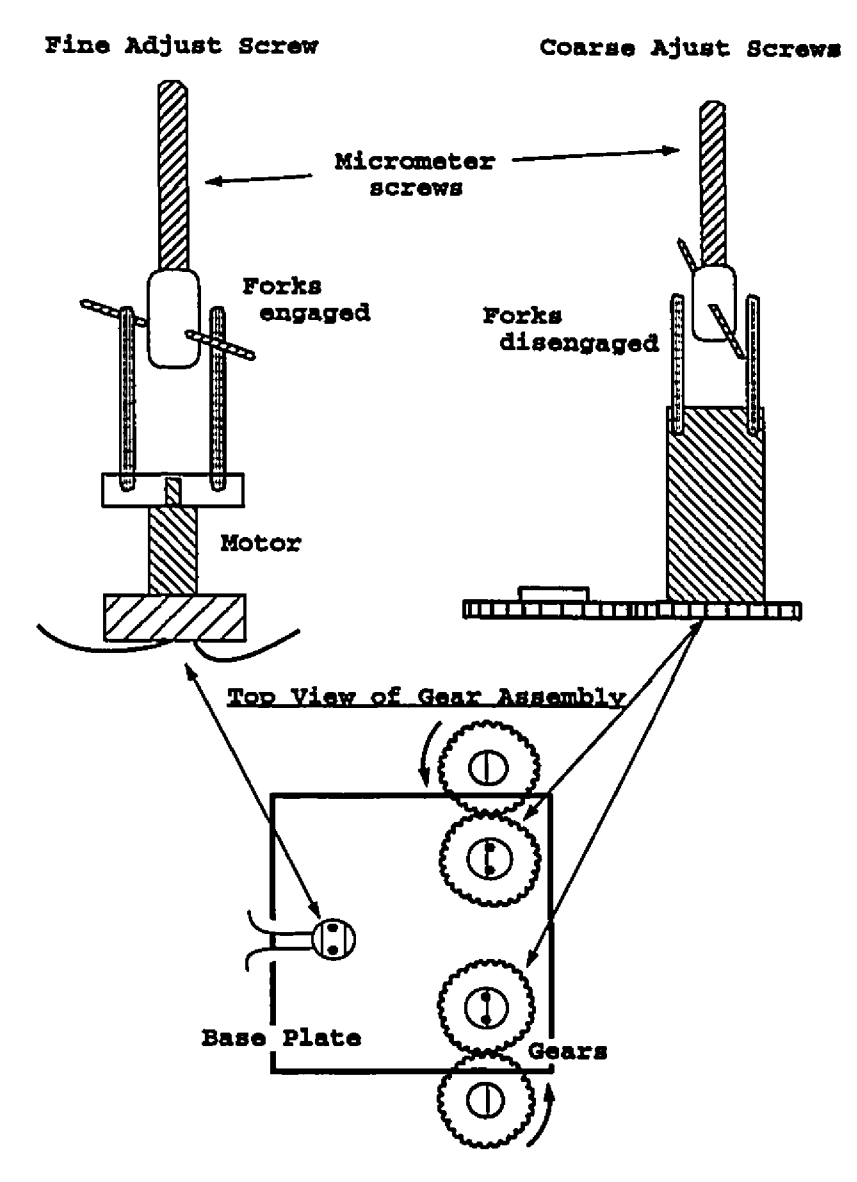


Figure 3.6: Micrometer screw adjustment on microscope is done by gears (in the case of the coarse adjust screws) or by a motor (in the case of the fine adjust screw). The motor has a 1024:1 reduction gear in order to provide fine motion. A fork-like connection is used so that the screws (fastened to the top damping plate) may be disengaged from the gears or motor (both fastened to the base plate) and so vibrations are not transmitted to the top damping plate. The fine adjust screw is shown here at the left with the forks engaged to the micrometer screw. The coarse adjust screw is shown disengaged. The top view of the base plate is shown at the bottom and includes the relative position of the three screws as well as their respective adjustment mechanisms.

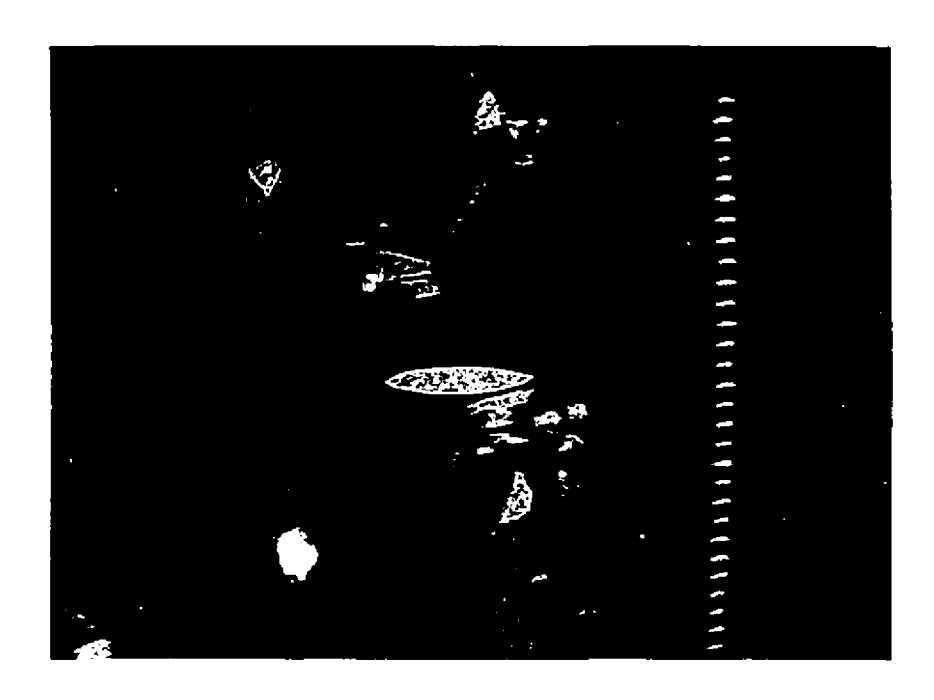


Figure 3.7: A closeup view of sample holder also shows the cantilever and the optical fiber chuck. The bimorph and the aluminum piece are also visible as is the micrometer screw that provides the coarse vertical positioning of the cantilever below the optical fiber.

disk, imaged on the scanner, then stored in a dust free environment when not in use. Many commercial instruments use a magnetic disk to affix the sample to. The sample is fixed to a thin disk made of a ferromagnetic, usually iron. The disk is attracted to a permanent magnet fixed to the scanner tube. We chose the set screw design over this simpler method since we intend to measure magnetic forces on our samples and a magnetic sample holder could introduce error in our measurements.

The sample is raster scanner under the control of the PC, which also collects the image data.

An additional stage was built by Mark Roseman to move the whole scanner by up to 8 mm. This "walker" uses a stick-slip mechanism to move two steel plates — one in each of the x and y directions — in steps of less then 100 nm. This has greatly increased our scanning range. We need now just to raise the cantilever, "walk" the scanner, and re-approach the tip in order to image a different section of the same sample without having to move the sample by hand.

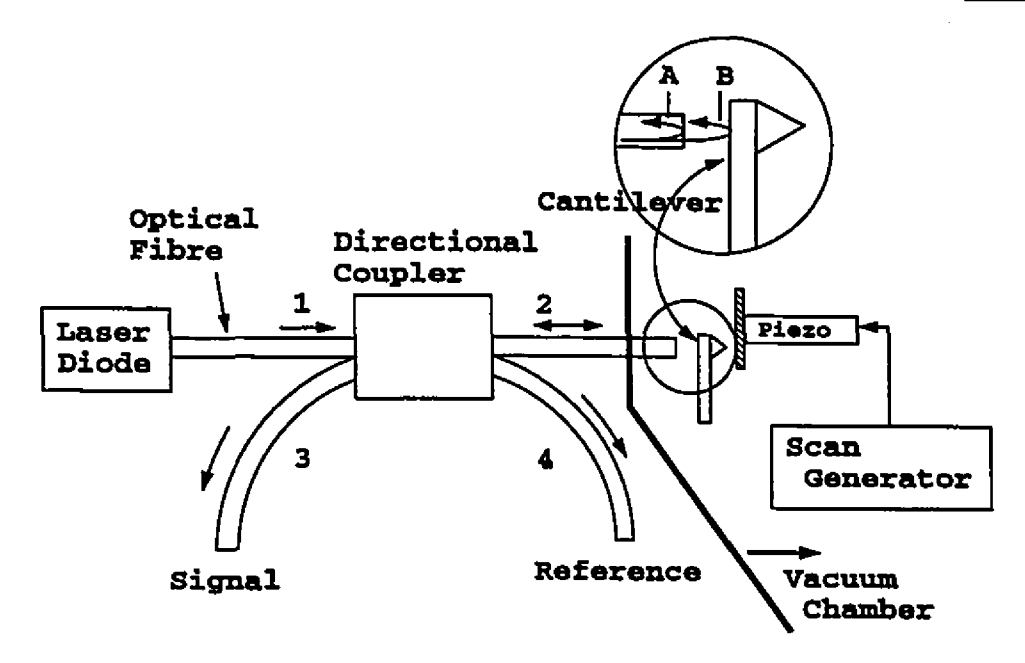


Figure 3.8: Laser interferometer

3.3 Fiber Optic Interferometer

We have chosen to use interferometry as opposed to beam deflection for our deflection sensor because of our focus on the force gradients of a surface and the ease of adapting such a system to vacuum and low temperature conditions. The laser interferometer is illustrated in figure 3.8. A semiconductor laser (we used a connectorized laser diode from Seastar Optics Inc. with a ILX Lightware LDX-3412 Precision Current Source) generates a 780 nm laser beam which is sent into a length of optical fiber. We used a 80 μ m outer diameter, 4.5 μ m inner diameter fiber optic cable made by 3M specially for transmitting at 780 nm. The beam follows path 1 and passes through a 3 dB bidirectional coupler (made by Gould Fiber Optics) which splits the beam into two¹. Half of the beam follows path 2 to the vacuum chamber where the tip of the fiber is brought to within 5 μ m of the back of the cantilever. At the fiber/air interface, about 4% of the original laser beam intensity is reflected back into the fiber (portion A), the rest escapes to reflect off of the cantilever and return (portion B) to the interface. Ideally², 4% of the original laser beam intensity re-enters

¹The cross-coupler is made by bringing the cores of two optical fibers close together. The evanescent field of the laser light is then shared between the two fiber cores.

²Only if the two interfering beams have the same intensity will the resulting interference pattern

the fiber. The two beams interfere with each other as they return through path 2 (the intensity of beam B is reduced to due to partial reflection at the cantilever and partial transmission at the fiber/air interface). The interfering beams pass through the coupler once more where one half of their intensity is directed to path 3. At the end of this fiber path, sits a UDT Sensors PIN-020A photodetector which records the interference signal and transmits it, as an analog signal, to the feedback electronics. Part of the beam also travels down path 4 and may be used as a reference signal to monitor the variations in laser output.

The interferometer is capable of resolving cantilever deflections of the order of 10^{-15} meters. Please see Albrecht, Grütter and Rugar [92], which contains a detailed description of the interferometer, and Rugar, Mamin and Guthner [89], which describes the performance of an interferometer similar to ours.

3.4 Vibration Damping and Noise

The level of background noise is of critical importance in every experiment. The noise considerations in the AFM are paramount and great lengths are needed to reduce these to a reasonable level. The best achievable noise level is set by the thermal vibrations of the cantilever, equation 2.6. Since these oscillations are of the order of 10^{-11} meters, it is a challenge to control all other noise sources and build a system dominated by thermal noise.

Every building floor typically vibrates at 20 Hz with amplitudes of several μ m. Together with the ambient acoustic noise from ventilation, people walking and talking, etc, the vibrations are a factor of 10^5 time larger than the cantilever deflections being measured. Fortunately, the vibration damping system doesn't have to cancel out all vibrations. As long as the microscope resonances are orders of magnitude larger than the external vibrations, such a stiff microscope will simply oscillate up and down with the external vibrations and not vibrate itself. Most of our microscope is built along those guidelines but since a few parts do have low resonant frequencies, extra

exhibit complete constructive and destructive interference, thus producing the greatest contrast.

measures are used to reduce the vibrations. First of all microscope rests on a vibration isolated workstation by Newport (model number M-VW-3660-OPT-02-10), where a heavy, honeycomb structured tabletop made out of steel is supported by four pistons. Each piston is damped by an air flow passed through a rubber diaphragm under the piston. The table is very effective at reducing the building vibrations, which oscillate the floors with micrometer amplitude at a frequency of under 20 Hz.

There are many vibration isolation mechanisms available to control the higher frequency vibrations. Many STMs use a magnetic eddy current damping system because of its vacuum compatibility and its easily varied damping coefficient. The damped metal plate stack was our choice for the AFM. Its response is described below (following the method by Okano et al. [87]). Another design involves suspending the microscope by elastic chords. This is a popular method since it provides good vibration isolation and is simple to implement. The response of the suspended system may be found in a number of references including Park and Quate [87] and Züger, Ott and Dürig [92].

The microscope sits atop a series of metal plates, separated by rubber spacers that serve to support the components of the microscope as well as dampen the acoustic vibrations that arise from various sources in and around the lab This damping stack is composed of a 25 cm X 25 cm, 1/4" thick stainless steel base plate and then 8 layers of thin and thick aluminum and stainless steel plates. The plates are separated by rubber spacers called grommets. Four grooves, one at each corner, were machined out of the metal plates so that the grommets could be inserted partway into each stack and thus provide not only vertical support, but also excellent lateral stiffness. It is actually difficult to nudge the plates by pushing them with your hand. (see figure 3.9 for diagram of the damping stack).

The final vibration isolation is done by evacuating the air around the microscope. The pressure is reduces to 10⁻⁴ Pa and since there are fewer molecules striking the cantilever, sound amplitudes cannot be transferred to the system. The greatly reduces acoustic coupling also, and more importantly, increases the quality factor of the cantilever by several orders of magnitude due to the reduced damping of the lever

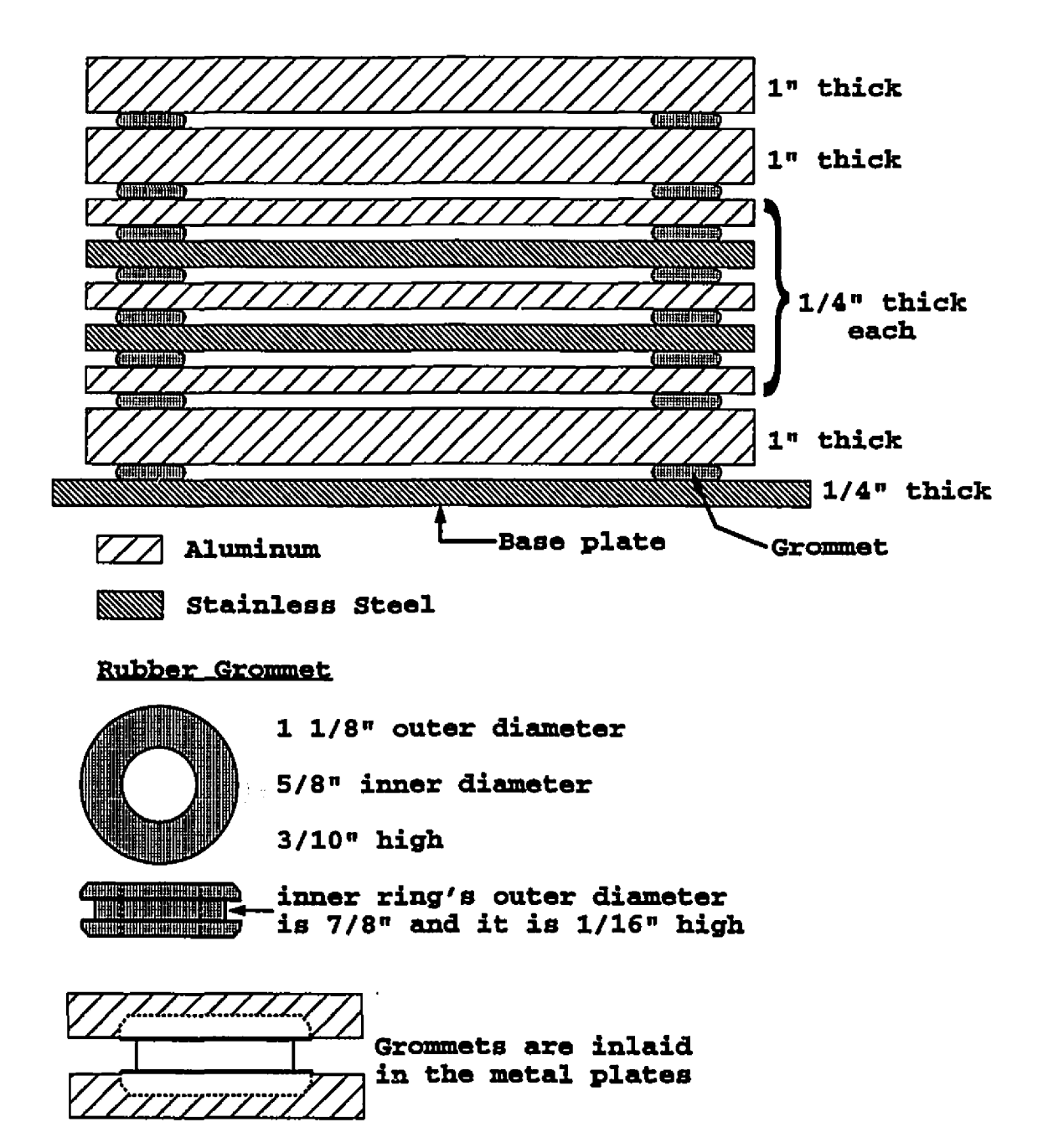


Figure 3.9: The vibration damping stack is made up of different thicknesses of aluminum and stainless street plates. The plates are separated by rubber grommets which are inlaid in the metal plates to provide lateral stability.

by the viscosity of the air. The air is evacuated using a Balzers TCP 121 turbo pump (the pressure is monitored by a Balzers TPR 010 Pirani Gauge and a Balzers IKR 020 Cold Cathode). Surprisingly, very little resonance effect arises from the turbo pump. We are able to keep scanning with no significant noise increase

The vibration stack can be modeled as a series of n coupled oscillators of masses $m_1, m_2 \ldots m_n$; spring constants k_1, k_2, \ldots, k_n ; and damping constant b_1, b_2, \ldots, b_n as shown in figure 3.10 where x_1, x_2, \ldots, x_n are the vertical displacements of the damping plates and $y = y_0 \cos(\omega t)$ is the displacement of the base plate which is due to external forces. The equations of motion for this system are:

$$m_1\ddot{x}_1 + b_1\dot{x}_1 + k_1x_1 + b_2(\dot{x}_1 - \dot{x}_2) + k_2(x_1 - x_2) = b_1\dot{y} + k_1y$$
 (3.1)

$$m_d\ddot{x}_d + b_d(\dot{x}_d - \dot{x}_{d-1}) + k_d(x_d - x_{d-1}) + b_{d+1}(\dot{x}_d - \dot{x}_{d+1}) + k_{d+1}(x_d - x_{d+1}) = 0 \quad (3.2)$$

where $d=2,3,\ldots,n-1$, and

$$m_n \ddot{x}_n + b_n (\dot{x}_n - \dot{x}_{n-1}) + k_n (x_n - x_{n-1}) = 0$$
(3.3)

The solution for n=8 plates is beyond the scope of this thesis (it is made even more difficult by the fact that the damping constants of the rubber spacers are frequency-dependent). The response of the plates was measured and the results are discussed below. The plates are doubly effective at reducing vibrations. We expect that the high frequencies are attenuated by the grommets whereas low frequencies are attenuated by the metal plates. Also, we expect that vibrations are reflected by the acoustic mismatch between the plates. Finally, not only are longitudinal vibrations suppressed, but the inlaid position of the grommets suppresses lateral vibrations as well.

The response of the damping system, the optical table and damping stack, was measured. The process involves aligning a cantilever with the optical fiber, placing the microscope head in different places and under different conditions in the microscope, and observing the vibrations of the cantilever. The signal from the photodetector is sent to a signal analyzer (Stanford Research Systems SR 770) where the spectrum of voltage versus frequency is recorded. In order to observe the damping efficiency more clearly, both the floor and the top of the optical table were excited, by jumping up and

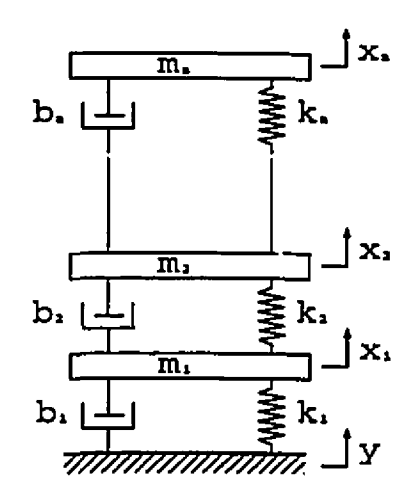


Figure 3.10: n coupled oscillators with spring constants and damping constants

down for the floor excitation and by tapping in the case of the table top excitation. This extra vibration source was necessary as we could hardly observe much damping with only weak background levels of vibrations.

First, we set up the worst-case scenario for vibrations. The microscope head was placed at the bottom of the vacuum chamber, shorting out the damping stack. Also, the optical table was left not floating and the top of the vacuum chamber was left open so that acoustic noise would be at its worst. By jumping up and down on the floor next to the microscope, we produced the top left noise spectrum in figure 3.11. The figure shows that large amplitude vibrations are present at low frequencies. There are two pronounced peaks in the spectrum. The first occurs at about 3 kHz and is a characteristic resonance of the bimorph. The second, broader peak occurs at about 31 kHz and it the resonant frequency of the cantilever itself. The best-case scenario was next. The top right spectrum in figure 3.11 shows the response of the system when the microscope head is now at the top of the vibration stack, the optical table is set floating and the vacuum chamber is under a high vacuum. We see that the low frequencies are still dominant but the bimorph resonance has disappeared and the cantilever resonance is narrower due to the increase in Q factor under vacuum. Notice that in both spectra, the amplitude rolls off with frequency. This is due in part to the 1/f noise of the system but is mostly an artifact of the photodetector and preamplifier which are more sensitive at lower frequencies. Since the signal analyzer actually measures voltage as a function of frequency, the conversion to Angstroms was done manually using a few hertz as the calibration frequency. The calibration rolls off very similarly to what is observed on the plots and so the high frequencies are actually constant in amplitude. By dividing the best-case by the worst-case, we can produce a transfer function showing the damping efficiency of the whole vibration isolation system. This is shown as the image on the bottom of figure 3.11. One problem that cannot be remedied at present is that the excitation frequencies and amplitudes are not reproducible. Since I am simply jumping next to the microscope to excite vibrations, the exact spectrum of excitation is not know, nor is it reproducible and very small changes in the location or enthusiasm of the jumping result in large changes in the response of the cantilever.

The transfer function shows that the damping is almost constant for high frequencies. Above 5 kHz, the system doesn't seem to be excited at all. This is probably because the microscope is built so stiffly that it is not possible to excite such high frequency modes with the current excitations. There is an odd-shaped bump at 30 kHz caused by the cantilever resonance which becomes narrower and goes up in amplitude under vacuum. The position of the resonance changes slightly under vacuum, so the dip in the transfer function is slightly off-center. It is clear from the transfer function that the low frequencies are more interesting and this is to be expected since the resonances of the floor and of the table top should be in the few to few hundred hertz region.

We can now narrow our focus and take a look at the frequencies between 1 and 200 hertz². Note that on this scale, the response of the photodetector is linear and so the vertical scale is accurate. First, we take a look at the efficiency of the optical

¹The photodetector signal is fed into an oscilloscope and a 1 kHz, 4 Volts peak-to-peak, signal is applied to the bimorph. The dc offset of the bimorph is adjusted to produce a symmetric oscillation pattern on the screen so now the cantilever is oscillating through fringes in the interference signal. The peak-to-peak voltage on the oscilloscope corresponds to a quarter of a wavelength of the laser light.

²We do not start at 0 herts since there is a large dc component to the photodetector that is constant on each spectrum.

5

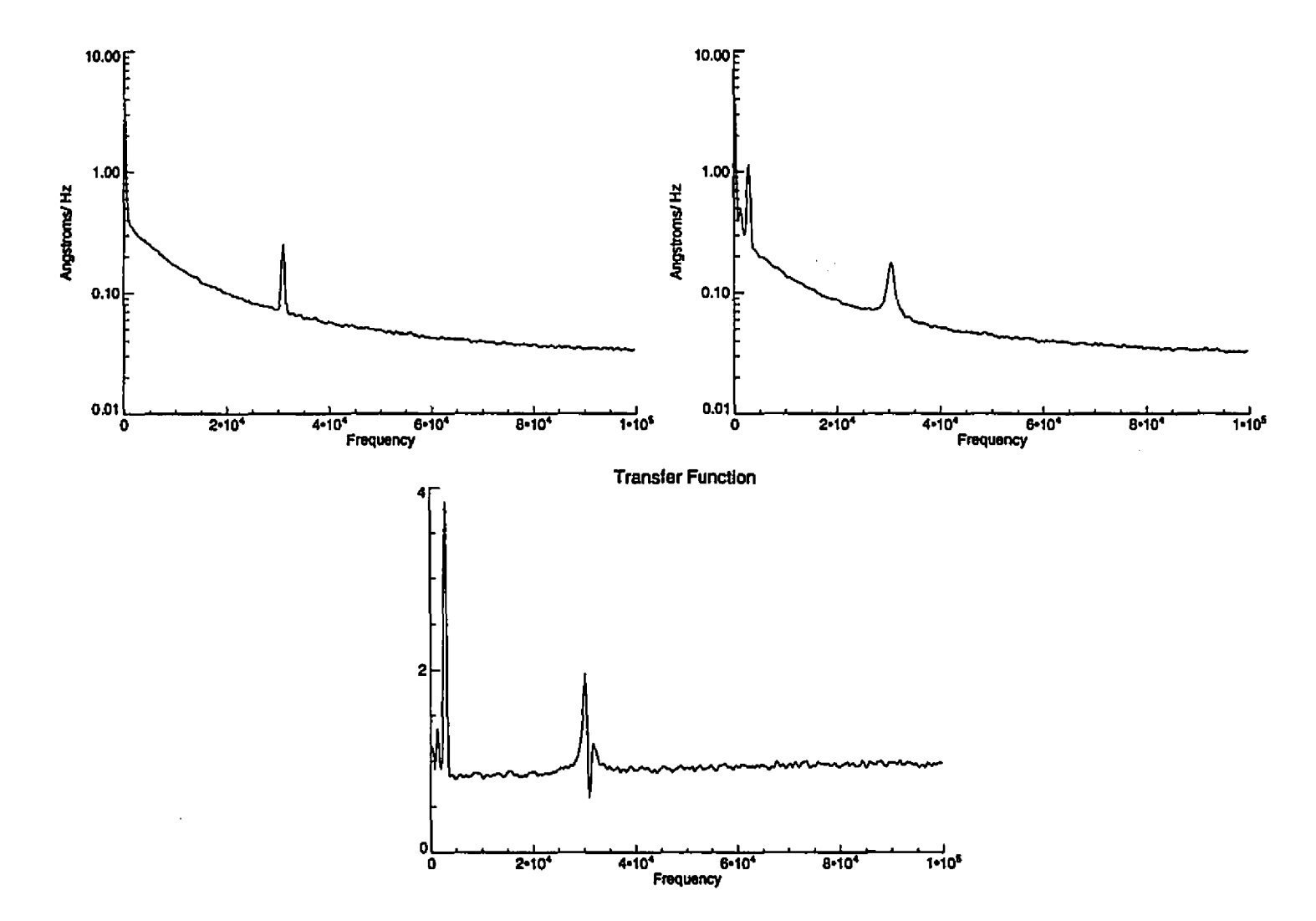


Figure 3.11: Noise spectra of microscope. The plot on the top left is a measure of the noise present when the optical table is not floating, the vibration stack is shorted, and the cantilever is susceptible to acoustic noise. The plot on the top right is a measure of the noise present when the optical table is floating, the microscope head is on top of the vibration stack, and the air has been evacuated from the vacuum chamber. The plot on the bottom is the transfer function obtained when the top left plot is divided by the top right plot. It shows the damping efficiency of the stack at high frequencies.

table. The top left plot in figure 3.12 shows the noise spectrum of the cantilever when the microscope head was placed at the bottom of the vibration stack, and the optical table was not floating. The jumping on the floor seemed to raise the background for most frequencies. The top right plot in figure 3.12 shows the noise spectrum when the table was set to float. Notice the pronounced peaks at 60 Hz and 180 Hz. These are caused by interference from the ac current from the wall sockets and every power source, motor and wire connected to it. The peaks are unusually prominent here, probably caused by the presence of a grounding loop since both the microscope head and the vacuum chamber are separately grounded. The 120 Hz peak, which is an odd harmonic of the 60 Hz fundamental, is missing which is a good indication of the presence of grounding loops since only even harmonics are present when there are loops. The transfer function is at the bottom on figure 3.12 and shows that the optical table has a damping efficiency of about 10 at frequencies below 100 Hz. Note that one advantage of scanning the sample rapidly, is that there is less noise present. We can see by the top right plot of figure 3.12 that vibration amplitude is less than 0.01 Aat frequencies above 10 Hz (this amplitude is even lower without the large external excitation of the microscope).

Now, let's take a look at the damping stack itself. The top left plot in figure 3.13 shows the noise spectrum of the cantilever when the microscope is placed at the bottom of the vibration damping stack, and the optical table was not floating. This time vibrations were excited by tapping the table top instead of jumping on the floor. This ensured that none of the resonant modes of the floor would reach the stack. This was, however, a very irreproducible way of exciting vibrations since even a slight touch of a wire on the table or one of the electrical feedthroughs of the vacuum system produced very different results in the noise spectra. The top right plot shows the noise when the microscope head is at the top of the stack. The transfer function is at the bottom and demonstrates that some damping is occuring though the exact amount is dependant of the excitation trial and even the frequencies change from trial to trial.

To observe the product of the optical table and the damping stack, we set the

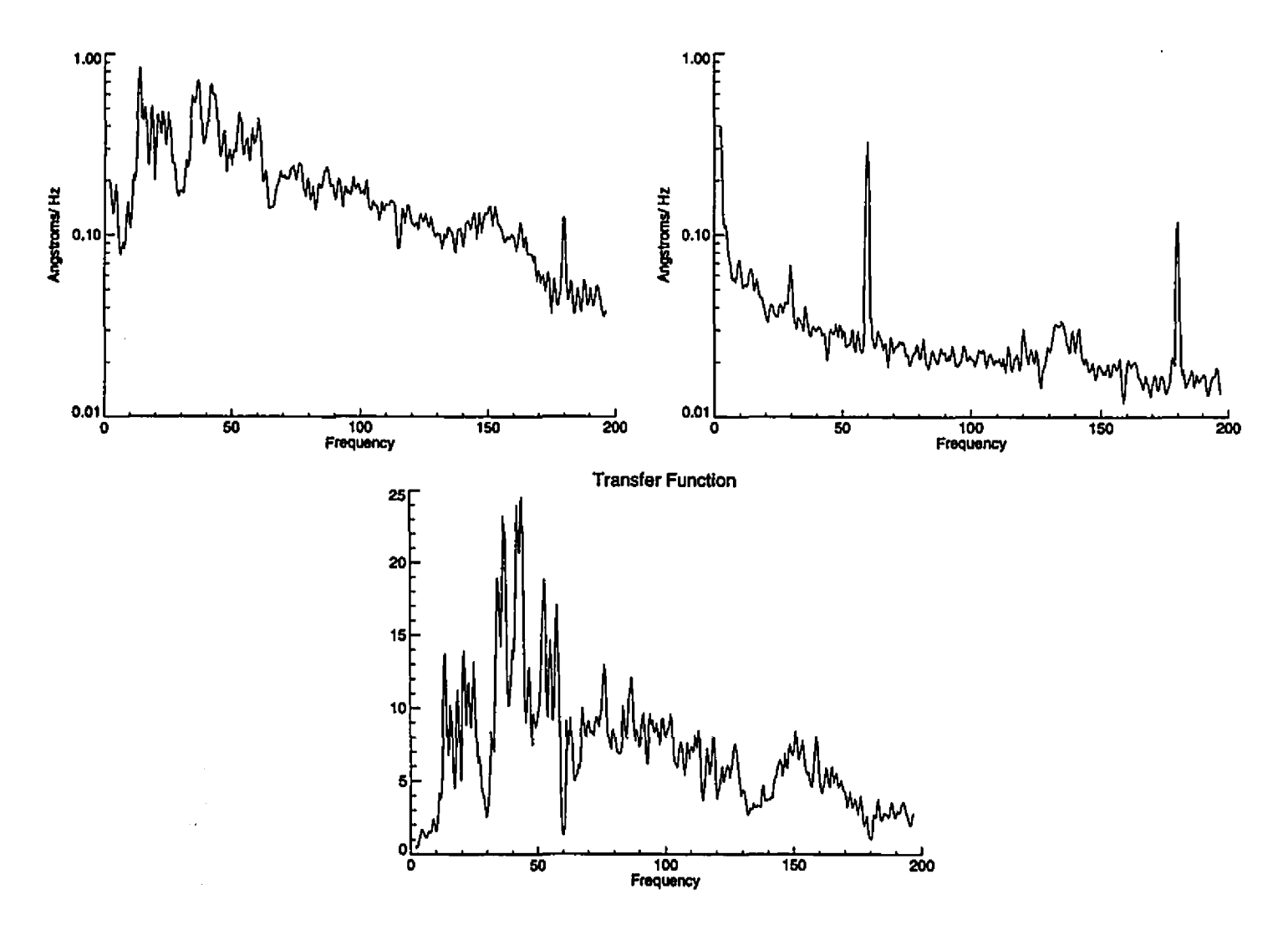


Figure 3.12: Mose spectra of microscope. For these three plots, the microscope head was placed at the bottom of the vacuum chamber and so the vibration stack was shorted. The top left plot shows the noise present when the optical table is not floating, whereas it is floating in the top right plot. The plot at the bottom is the transfer function obtained by dividing the top left plot by the top right one. Notice that the damping efficiency drops to 1 at 60 Hs and 180 Hs. Since these are not resonant frequencies of the table, but rather are electric in origin, the fact that they have the same amplitude in both plots is a check to assure that the noise measurements are valid.

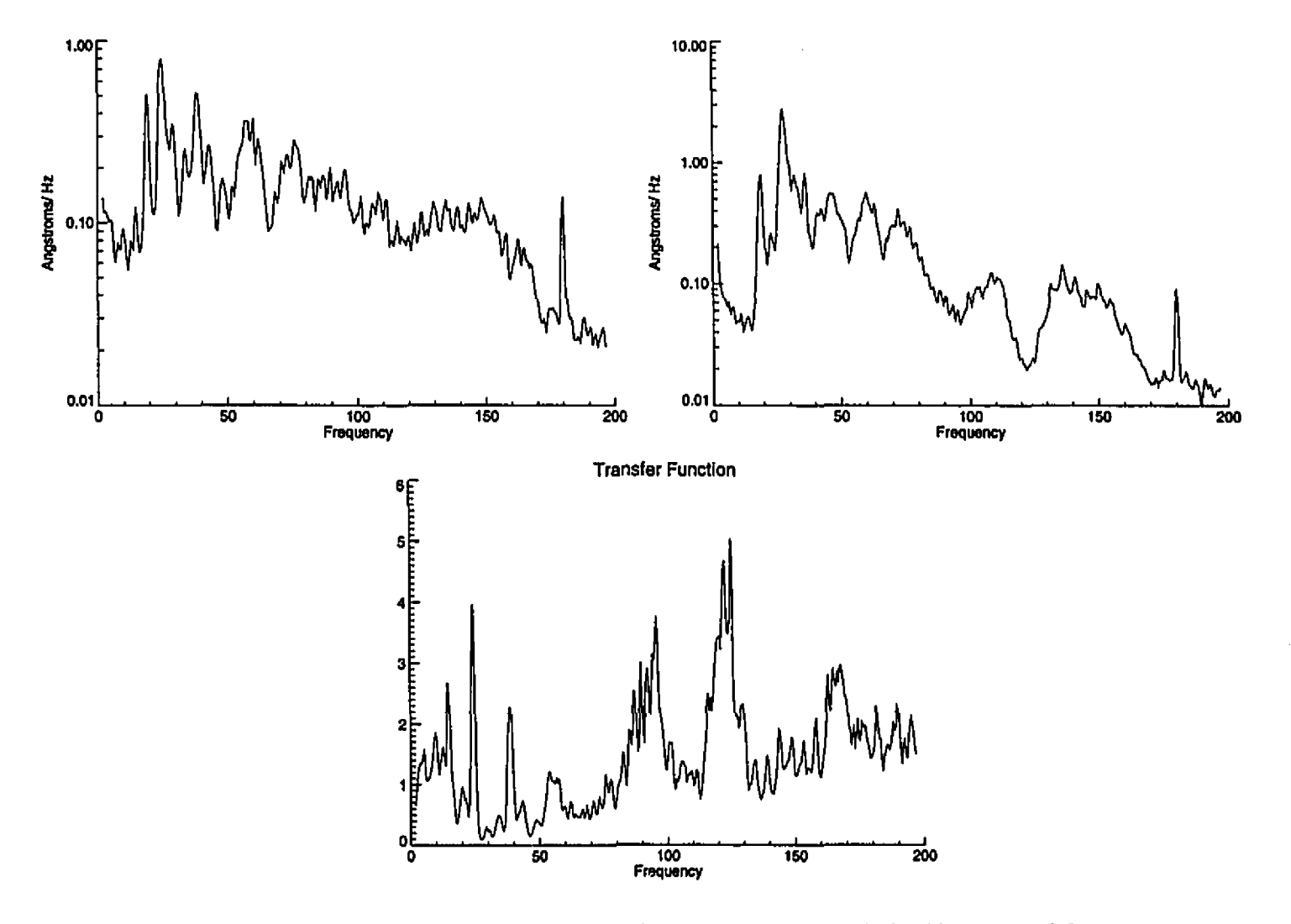


Figure 3.13: Noise spectra of microscope. For the three plots, the optical table was top left not floating and the only the table top was tapped by hand to provide the vibration excitation. The top left plot shows the noise distribution when the microscope head is placed at the bottom of the damping stack. The top right plot has the head on top of the vibration stack and the bottom plot is the transfer function obtained by dividing the top left plot by the top right plot.

table to floating and repeat the same steps as for figure 3.13. The transfer function is figure 3.14 is measure of the efficiency of the whole stack. Note that the amplitude is not the true damping efficiency of the stack since we could not reproduce exactly the same excitation conditions and the spectra are vastly different for slightly different excitations. Even the location of the peaks is different from trial to trial.

The result of the vibration measurements is that the optical table and vibration damping stack provide some vibration isolation for the microscope although even a qualitative discussion is difficult since the magnitude and frequency of resonant frequencies are different for each scan. The optical table seems to function best at frequencies below 100 Hz, the vibration stack working above 100 Hz. The microscope itself seems to have a large dynamic range. When two people jumped up and down instead of one, the noise level at the top of the vibration stack remained constant even though the excitation at the floor doubled. A more precise and reproducible method of excitation is required for more details.

3.5 Electrical Connections to Microscope

Electric cables connect to the microscope to control most of the positioning, including the motion of the scanner and the bimorph, as well as operate other devices such as the electromagnet. Though they are vital to the operation of the microscope, the wires must be properly connected to avoid problems. There are three major effects from the electrical connections. The most obvious is the pickup of ambient electromagnetic radiation by the cables. This is made worst by the fact that the physics department is downhill from a series of radio and television antennae and next door to a large electric transformer station. The second effect is the presence of grounding loops in our connections. Electrical circuits work best with a single ground point, if more than one grounding path is present, the circuit will tend to resonate or exhibit some interference. The final effect is that wires leading directly to the microscope are capable of carrying physical vibrations. If not properly fixed down, the wires may bypass the vibration damping systems and carry vibrations directly to the sample or

17

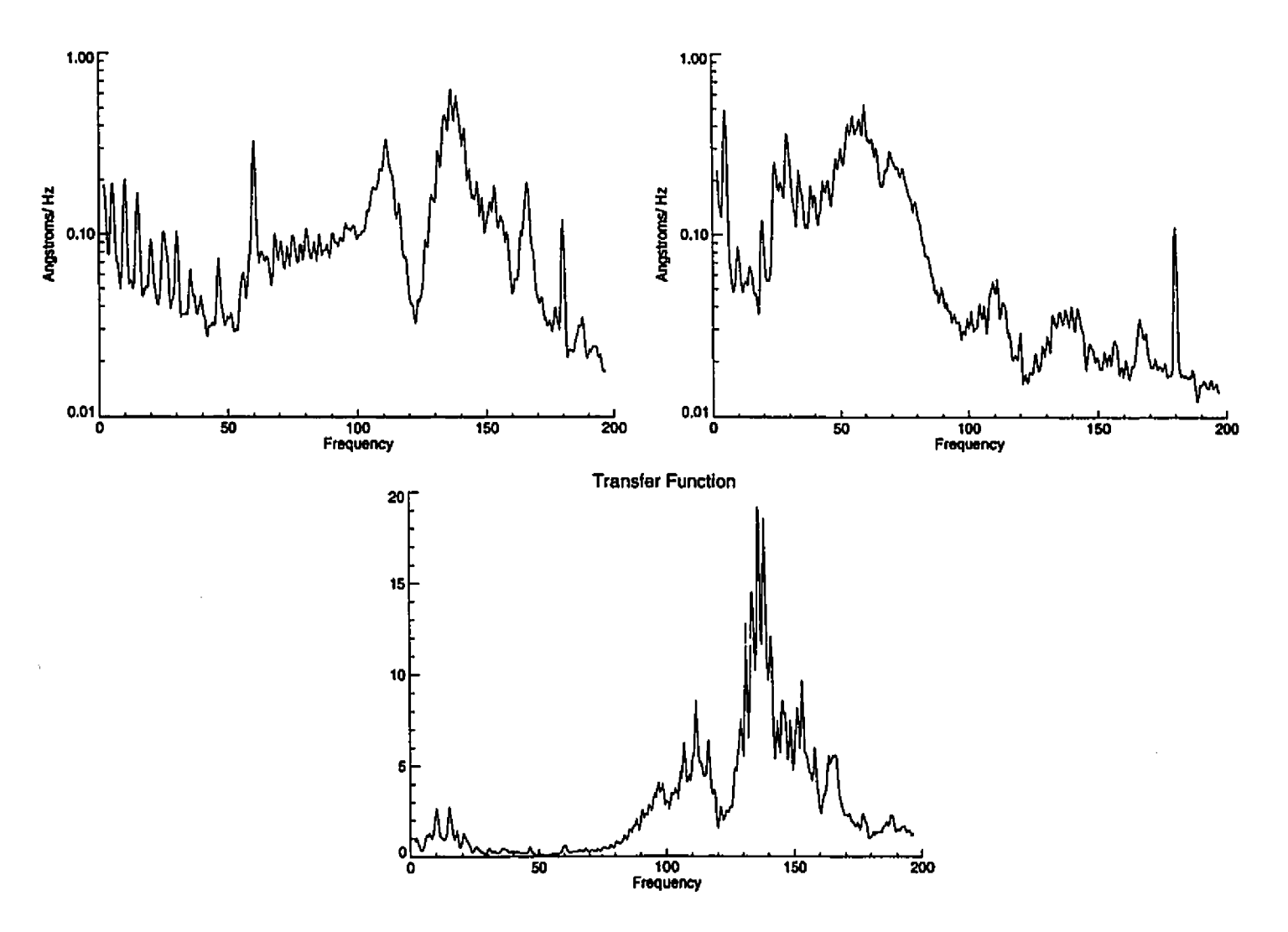


Figure 3.14: Noise spectra of microscope. For the three plots, the optical table was floating to provide a measure of the combined damping of the optical table and of the stack. The top left plot shows the noise distribution when the microscope head is placed at the bottom of the damping stack. The top right plot has the head on top of the vibration stack and the bottom plot is the transfer function obtained by dividing the top left plot by the top right plot. The damping seems greatest above 100 Hz but the true spectrum is a function of the excitation spectrum.

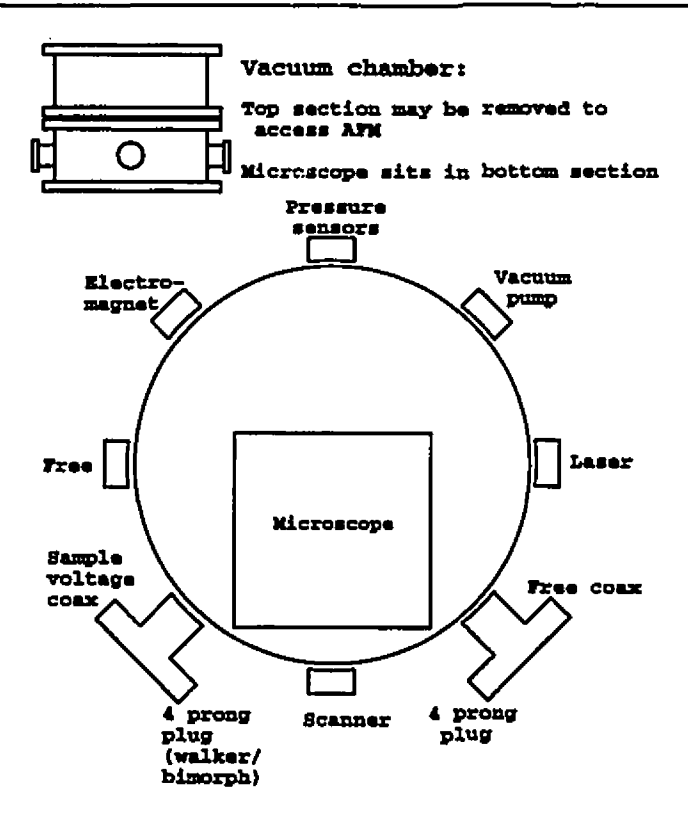


Figure 3.15: Electric feedthroughs to vacuum chamber. The microscope sits in the bottom half of the vacuum chamber and is connected to the outside by wires connected to the vacuum feedthroughs.

to the cantilever. Through the use of proper shielding, we have been able to eliminate electronic interference as a major source of noise. After eliminating a few loops, the grounding of the microscope seems to be in order as we don't observe any 60 Hz signal.

A number of steps were taken to isolate the microscope from the vibrations carried by the wires. First, the wires are bolted to the optical table. The small mass of the wires is not able to vibrate the heavy table. Second, the wires are connected to a series of feedthroughs on the vacuum chamber (see figure 3.15). From the feedthroughs, the wires are connected to an electrical connection plate which is screwed into the base plate of the microscope. The wires then pass up the vibration damping stack to another electrical connection plate screwed to the top plate of the stack. The connection plates are aluminum with cut-outs where a piece of prepunched perfboard is screwed down. Integrated circuit connectors are soldered to the perfboard and the electrical wires are soldered to pins that plug into the connectors. As they pass up

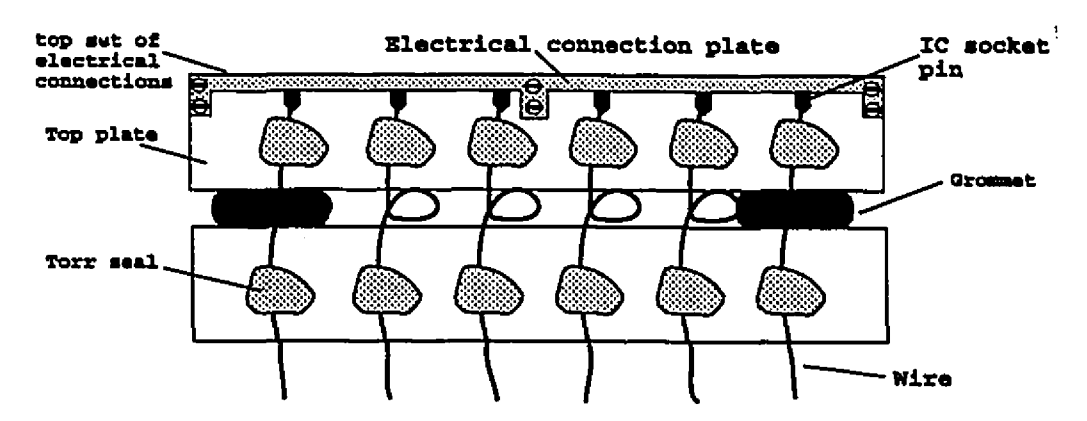


Figure 3.16: The twisting and mechanical fixing of wires provides vibration isolation. Vibrations carried by the wires are damped by the vibration stack. The wires are glued with epoxy to one plate, then a small loop is made and the wire is glued to the next plate. The loop is so that the wire does not interfere with the damping motion of the plates. The wires are connected to the top and bottom of the stack by being soldered into integrated circuit sockets.

the damping stacks, each wire is attached to each damping plate. To do this, each wire is fixed to each plate with vacuum-compatible epoxy¹. A small loop is then made with the wire and the end attached to the next plate (see figure 3.16). The epoxy attaches the wire to the plates so that they don't interfere with the plates' damping mechanism. The loop serves to let the damping plates act without shorting vibrations from plate to plate through the wire. The wires are finally inserted into the fixed top connection plate from where they are connected to their final components, vibration-free.

This modular construction makes for quick repairs and easy installation of new components (magnets, electric heaters, etc) to the microscope. See figures 3.17 and 3.18 for the electrical connection diagrams. The modular construction of the damping plates and the wiring was put to the test while I was writing this thesis. Due to an accident, one of our samples fell off the sample holder and fell through the micrometer screw hole to the bottom of the stack. By unscrewing the bottom electrical connection plate, then lifting up the whole vibration stack and microscope head, we found the sample and were ready to scan again only a few minutes later.

1

This is a long process of fixing each wire first with cyanoacrylate glue (such as Krasy GlueTM), then spreading the epoxy (such as Torr SealTM) evenly and neatly so that it doesn't interfere with the other wires or the other damping plates. A hot air gun is used to heat the epoxy until it glistens. This helps to cover the wires evenly, improves bonding and speeds the hardening of the epoxy.

Four connections (alternating connected then non-connected starting with first pin) Scanner: X-walker SMC connections bimorph +X -X +Y -Y +Zy-walker (left one is used for sample voltage) bimorph-ground Top plate Y-ground X-around Not connected ground for walker for walker

Figure 3.17: The top set of electrical connections are screwed onto the top damping plate. The connection diagram is shown here. Only the top row of the IC connectors is used. Each IC connector's bottom row has all its pins soldered together to provide support. The first connector is reserved for the sample scanner. The second is free at the moment and has four connections, with the sockets alternating connected then not-connected, starting with the first pin. The next two connections are for SMC connectors (the first one is used for applying a sample voltage, the other is free). The final IC connector is used for the scanner walker connections as well as those going to the bimorph and the common ground of the top damping plate.

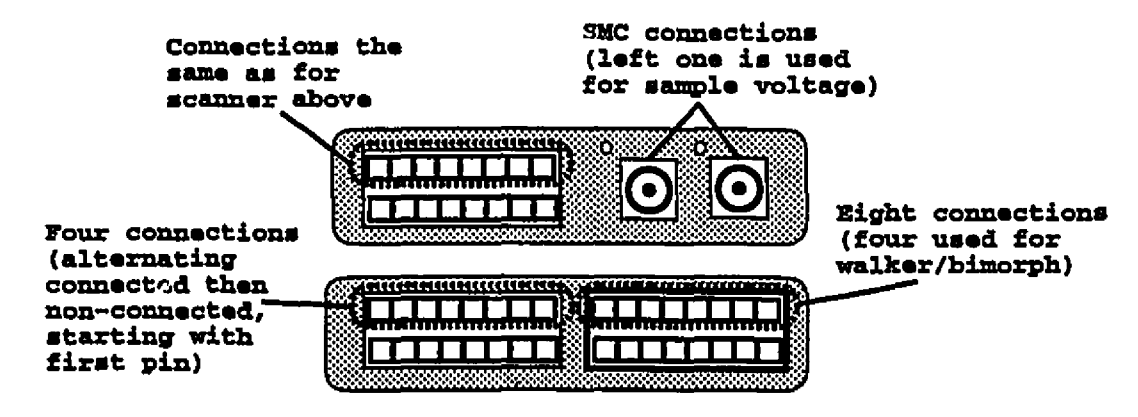


Figure 3.18: The bottom set of electrical connections are screwed to the base plate. They are connected identically to the top set of connections except that the top row is now soldered together for stability instead of the bottom row.

3.6 Electromagnet

One of the exciting field in AFM is the study of magnetic samples. The cantilever tip is covered with a magnetic coating so as to be sensitive to the magnetic stray field emanating from the sample. Magnetic Force Microscopy will play a major role in my future studies here at McGill starting with the study of the interaction between microscopic magnetic domains.

To more deeply understand magnetic phenomena, it is practical to be able to apply an external field to the sample. For this, we developed an electromagnet to be integrated into the vacuum chamber of the microscope. Since the first materials we will be looking at have rather small coercivity, H_c , a magnet with a peak field of 1 kiloGauss was judged to be sufficient. We decided to build an electromagnet, as opposed to say a rotating permanent magnet¹, for its simplicity of design and operation. Electromagnets with magnetically soft cores also have, usually, lower remnant fields in the gap then the other magnet designs. I found out that the simple idea wasn't as simple actually to build as I had hoped.

I used magnetic steel as the core for the magnet. The magnetic core enhances the field of the solenoid winding around it and that material was readily available in the machine shop. The first design for the electromagnet was a horseshoe form with two small poles and the winding at the middle of the yoke. Straight pieces of steel were machined, then screwed into one another to form the horseshoe. The winding was done with a 19 gauge (0.91 mm diameter) wire tightly wound, row after row, on a lathe². This prototype needed more than 7 Amps of current to achieve a 1 kG field and the wire reached a temperature of more than 180° C. By sprinkling a layer of iron filings on top of a plastic board which covered the magnet, a profile of the magnetic

¹see Cugat, Hansson and Coey [94] for look at a variable flux source composed of four rotating cylindrical magnets.

²The lathe winding of the electromagnet core is done by placing the rod in the lathe chuck, then two thin disks are placed apart on the rod and held in place with set screws. The disks act to define the width of the core winding so that the core is nice and cylindrical instead of being flattened at the ends. The wire is taken from a large spool resting on a support so that it can turn quickly as the lathe turns.

field was obtained showing where the field was the strongest and what orientation the magnetic flux had around the magnet. It was apparent that the flux escaping from the screwed-in corners of the magnet was comparable to the flux in the air gap¹. Something had to be done.

For the next prototype, we noticed that if we used a smaller diameter wire, that we could increase the number of amp-turns (since more turns of wire could fit in the volume available) and also reduce the power that needed to be dissipated by the magnet since we could reduce the current and generate the same magnetic field². Since we are practically limited by the winding techniques (can't put too much strain on a very thin wire as you wind it on the lathe) and by the power source needed (the voltage needed across the wire gets quite substantial for very thin wires), a practical limit is imposed. I was now winding with a 29 gauge (0.29 mm) wire and was determined to make the magnet out of a single piece of steel to reduce the flux leakage from the corners. First, I tried winding the magnet yoke then bending the the magnet into shape with a vice used to bend concrete reenforcement bars. The vice wasn't strong enough to bend the diameter of steel that I was using. For my next attempt, I took an acetylene torch and bent a steel rod into the "U" shape, wound the core on the lathe (this took almost two hours) and then torched the ends of the U-shape inwards to form the poles of the magnet. It took a few tries to align the poles correctly without burning the wire or myself. Finally, the magnet was ready but when plugged into the power supply, I discovered, to my infinite exasperation, that the flux leakage from the corners was nearly the same as it had been for the assembled magnet.

¹A difficulty that I faced with the design was that the separation of the poles was to be 2 cm. This is comparable to the pole diameter since the magnet is constrained by having to fit between the microscope head and the top damping plate. The large pole separation means that a lot of magnetic flux will leak out anywhere it can. This was a problem with all the horseshoe prototypes I built in that large amounts of flux always leaked out of the bends in the magnets.

²The current needed for a constant field divided by the power dissipated by the wire goes as a constant times the radius of the wire (the constant is proportional to the thickness of the windings and inversely proportional to the radius of the core). Since this is linear in radius, a thinner wire requires less current to generate the same magnetic field.

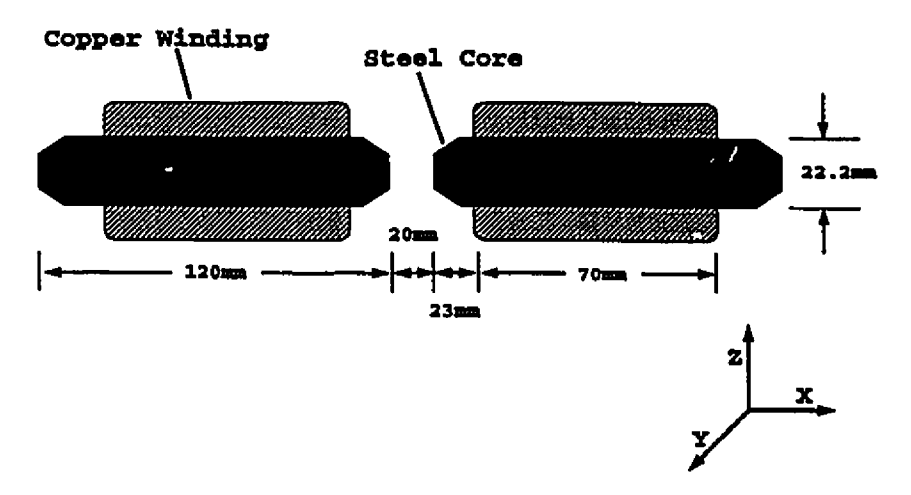


Figure 3.19: Electromagnet designed for our AFM. The steel core is wound with 10000 turn of copper wire. The coordinate system was used to produce the plots in figures 3.20 - 3.21.

The final design for the magnet, seen in figure 3.19, is simple, easy to construct and takes very little time to wind. The core is made of cold rolled steel (make number C-12L14), which was used because it is magnetically soft, is easy to machine, and is readily available in our machine shop. The two pole pieces are 12 cm long and tapered at the ends to enhance the flux density in the gap. A 1 kG field is easily attainable with only 0.215 Amps. Each pole piece is wound with 10000 turns of 32 gauge (0.22 mm) wire. There is an electrical tape layer between the wire and the core to prevent any unfortunate shorts and another layer surrounding the windings to insulate from electrical shock as 210 Volts are needed to provide the needed current (the resistance of the wire is 975 Ohms). Each pole can be adjusted independently about the sample and the gap widened for larger samples if needed. The remnant field in the gap is at most 12 Gauss in any direction. The magnet gets pretty warm when ramped up to 1 kG field, reaching a temperature of 60° C after an hour where the temperature levels off, increasing very slowly. The magnet is tapered at both ends to increase the flux density. Also, the winding is centered to one side of the magnet so that the magnet may be reversed to accommodate larger samples or another device placed about the sample, such as a heater. We are actually planning to have two separate magnets (four poles) in some experiments so that the magnetic field may be adjusted in any direction in the plane of the sample. The magnetic profile in the gap of the electromagnet is shown in figures 3.20 and 3.21. The electromagnet was laid out on

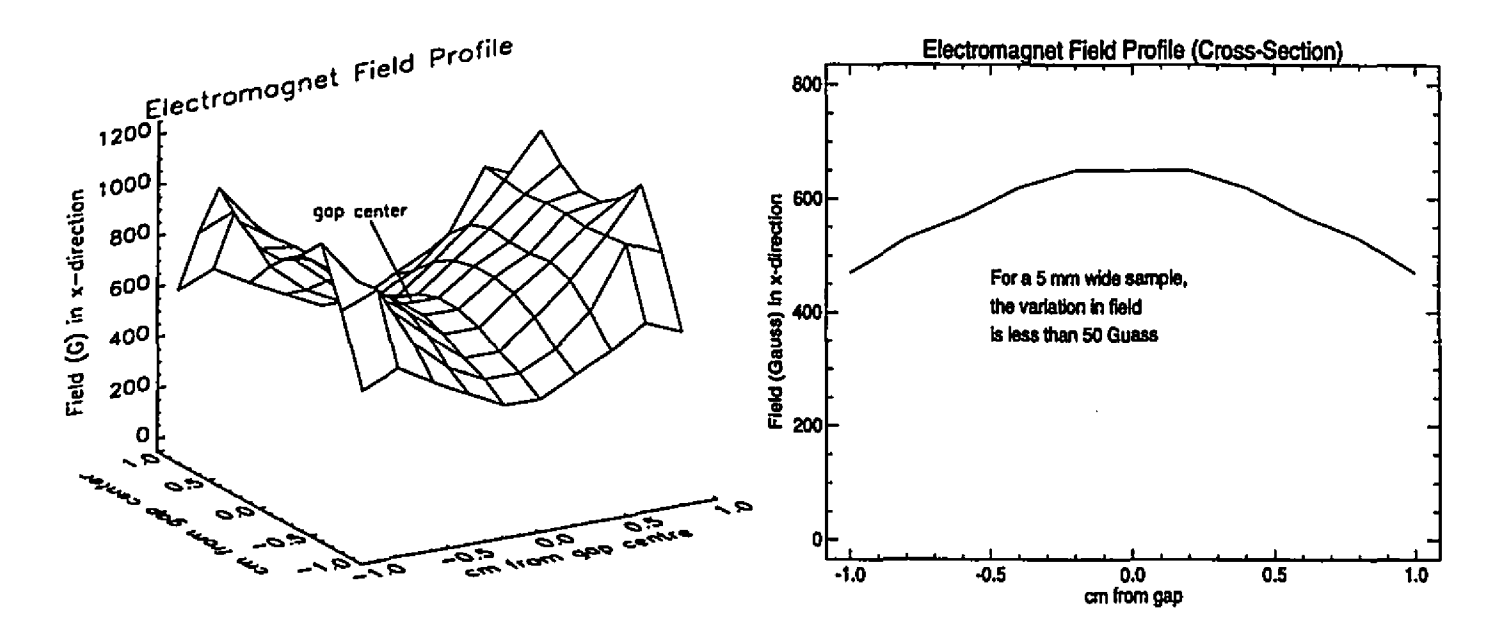


Figure 3.20: Magnetic field in x-direction in the air gap of the electromagnet. In the top left plot, the magnet poles are at x = -1.0 and x = +1.0. The two field spikes visible near the center of each pole are due to the flux leaking out of the corners of the pole tapering. The right plot is a cross-section of the field at the very center of the gap.

a table with a gap separation of 2 cm between the two magnet cores. The leads were hooked up to a power supply which provided 0.139 Amps to the magnet, producing a magnetic field of 650 Gauss, directed along the axis of the magnet, at the center of the gap. A tesla meter was placed at the center of the gap and scanned in a plane to probe the magnetic field in the gap.

Figure 3.20 shows that the magnetic field along the axis of the electromagnet varies smoothly across the gap. The field drops off rapidly. At the very center of the gap, the field is only 65% of the field at the poles. The right plot in figure 3.20 shows that at the center of the gap, the field is relatively constant. A 5 mm wide sample, placed at the center of the gap, would experience a variation of less than 50 Gauss across the sample.

The magnetic field in the direction of the axis of the electromagnet is not the only field present. The actual field on a sample is the vector addition of the fields along all three dimensions. Since the magnet exhibits cylindrical symmetry, only the x and one other dimension, say, the z-directions are of interest. Figure 3.21 shows

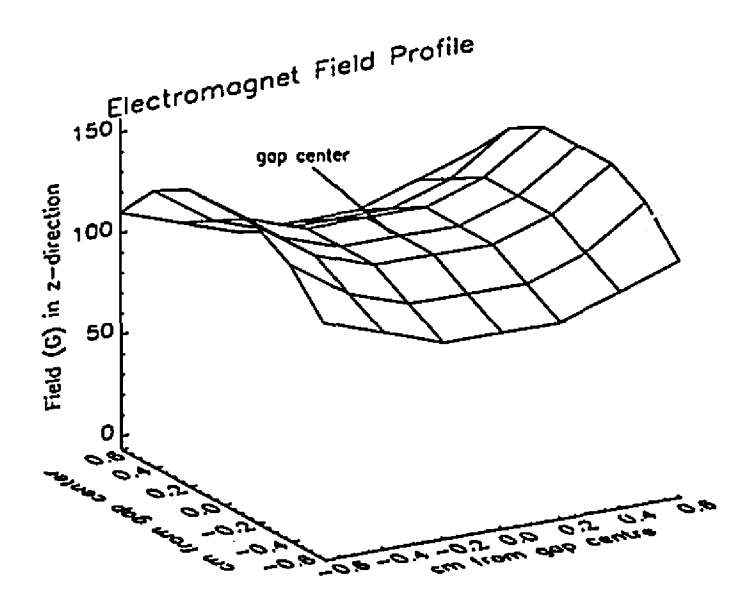


Figure 3.21: Magnetic field in z-direction in the air gap of the electromagnet. The plot was obtained similarly to the top left plot in figure 3.20 except that the tesla meter probe was rotated to measure field in the z-direction.

the field profile, in the gap, in the z-direction. The field at the center of the gap is only 110 Gauss and varies by less than 30 Gauss across the gap, even near the poles. Samples placed in the gap would thus be much more influenced by a variation along the x-direction than along any other axis.

3.7 Data Analysis

The data goes through many stages from acquisition to final image (see figure 3.22).

The interference pattern incident onto the photodetector is converted to an analog current and is passed to a pre-amplifier and a bandwidth filter. The amplified and filtered signal serves as input to a digital signal processor (DSP) made by East Coast Scientific (the signal may first be analyzed by either a lock-in amplifier or a phase locked loop, both of which determine its frequency and phase). The first component of the DSP is a 16 bit analog-to-digital converter (ADC), then there is the digital processor itself (which actually sits in the computer) and finally, a digital-to-analog converter (DAC). The DSP generates the scan of the sample. It also provides the

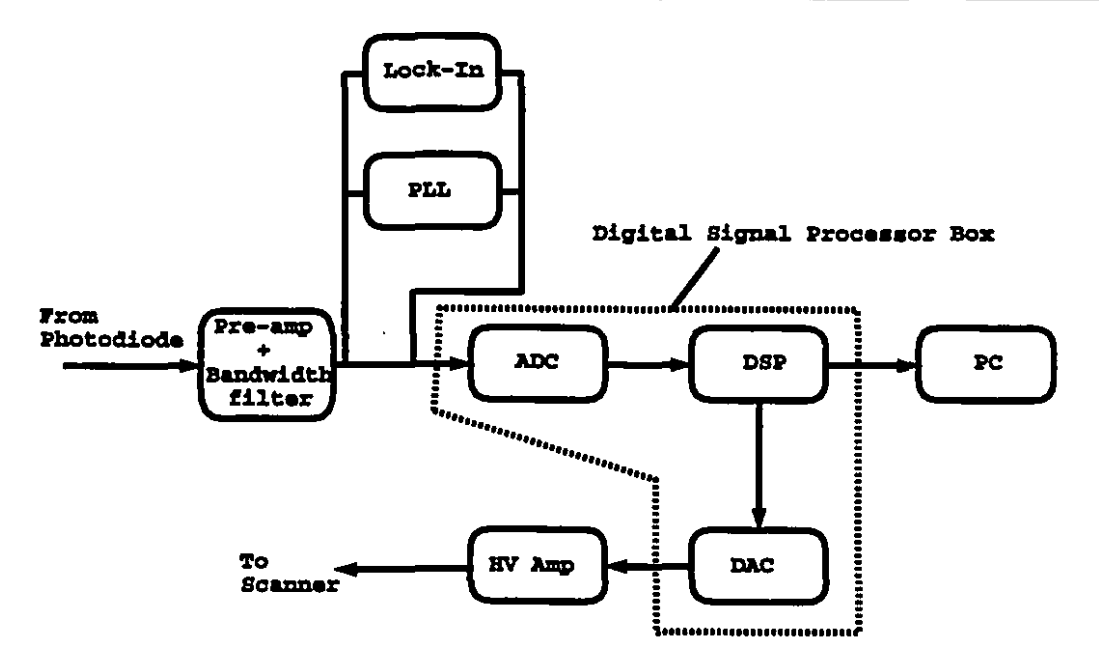


Figure 3.22: Path of data through the microscope

feedback signal (which controls the vertical position of the sample under the cantilever) to the DAC (which moves the piezoscanner), and transfers the image data to the computer. Our feedback happens to be done digitally, but this is not the case for all microscopes.

The data acquisition program contains the operating parameters of the DSP. It also displays the images and has a few image analysis functions. The scanning program we are using is called SPM version 4.4 by East Coast Scientific. The bulk of the image analysis is done from our Silicon Graphics INDY¹ To analyze the image, we use a program called SXM² which is a graphical user interface shell built on top of the main analysis program, PV-WAVE version 4.2 by Visual Numerics. SXM is copyright from the University of Basel, Switzerland and was programmed by D. Brodbeck, D. Buergler, R. Hofer, and G. Tarrach. It has most of the image processing operations of PV-WAVE that are commonly used by SPM scientists.

I Invite you to visit our lab at McGill University for more details on the microscope and on the SPM group.

¹See appendix A.1 to see how the data is transferred to the INDY.

²SXM is short for Scanning X Microscopy where X can be F for force, T for tunneling, etc.

Conclusion

Atomic Force Microscopy is a powerful tool for the challenges ahead in science and technology. Our AFM is designed to be easy to operate, is sensitive enough to measure small forces on a variety of samples, and is modular in construction to provide quick repairs and effortless addition of new components to the microscope.

Both coarse and fine adjustment controls enable fast and accurate positioning and control of the interferometer, the cantilever and the sample. The coarse adjustment controls include micrometer screws, a dc motor, and gears turned by hand. The fine adjustment takes the form of a piezoelectric positioner and special care must be taken to properly consider their effects on the final image.

The vibrations present in the lab are, for the most part, at frequencies too low to excite any vibrations in the microscope and thus don't affect our scans. Special measures have been implemented to reduce the effect of the vibrations which do affect the microscope. Vibrations below 100 Hz are attenuated by the optical table. Those above 100 Hz are attenuated by the damping stack which uses both rubber grommets and different sized metal plates to absorb and reflect vibrations.

An electromagnet was built to aid in the investigation of magnetic effects on a sub-micrometer scale. The electromagnet is made of two cylindrical steel cores with 10000 turn of winding each. A field of 1 kG in the center of the 2 cm air gap is easily obtained without causing the magnet temperature to increase substantially.

IMPOVEMENTS AND SUGGESTIONS

5.1 Improvements

?

It would be possible to greatly improve the magnetic field of the magnet by a suitable choice of magnetic core material. The low permeability of the steel that we are currently using ($\mu_r \sim 5$) makes for an inefficient magnet. A company that has quoted me a value of $\mu_r = 100,000$ for their special brand of electromagnetic iron. With this as a core, we would be able to generate a 1 kG field with a small fraction of the current and thus use much less power. Alternatively, we would be able to generate a maximum field of around 15 kG (the saturization magnetization of the iron) instead of being limited by the power dissipation of the magnet.

It would also be possible to wet-anneal the magnet core at 1200° C in a hydrogen environment. This should improve the permeability and reduce the remnant field.

The cantilever holder we are currently using is rather awkward. A more simple design involving a small fastening clip is used in the commercial NanoscopesTM. A similar design would make for a much easier, more reproducible cantilever-fiber alignments and probably increase the Q-factor of the cantilever.

We would be able to measure the transfer function of the vibration damping stack accurately either with a device capable of reproducing excitation spectra (like a thumper) or with the use of a second interferometer. One interferometer could be placed at the top of the damping stack, the other at the bottom and a transfer function independent of the excitation spectrum could be obtained.



The data analysis software we use is very powerful but the data acquisition software could use some improvements. It is not user-friendly and still has a number of bugs even after multiple versions. With repeated use, it should become easy to operate but for future instruments, more powerful software should be investigated.

5.2 Suggestions

What at first seems like a long job usually turns out to take less time than trying many different shortcuts, and also usually a better job is done by just setting your mind to it right away.

I strongly suggest that people handling Krazy GlueTM be very careful. The stuff instantly bonds to skin and can be dissolved with acetone though this is not an option if you get it near your eyes. There is a tendency when handling wires that you glue yourself to the wire and in the process of separating the wire and your finger, you either rip the wire, rip a connection, or often rip the insulation off the wire. Using tweezers or a toothpick is less dangerous to the wire.

I suggest that when designing a part to be machined, plans should be carefully drawn and kept as a record. If you design as you go, my personal favorite, measure the final piece. The addition of new parts to the microscope is much easier with an accurate diagram including the dimensions.

The magnet design deserves some scrutiny. It would be interesting to see what the relationship is between the field strength in the gap of the pole and the angle of the pole tapering, now set at 30°. A more gentle slope will decrease the amount of flux lost but you also lose core material. Round corners could be made instead of the sharp one now used but it isn't clear to me if a comparatively long curved section leaks more than an abrupt and final change in angle.

Don't eat worms.

APPENDICES

A.1 Data Transfer from PC to INDY

A sample image, once saved as a IMG format from the data acquisition program, is transferred from the PC to the INDY by an Ethernet connection over the physics department computer network. The simplest way to do this is by using File Transfer Protocol (FTP). The INDY is addressed as *luthien* (a character from *The Lord of the Rings*) and the PC as *cameleon* (we have a large multicolor chameleon Swatch poster next to the computer). Both reside at *physics.mcgill.ca*

From any directory on the PC, preferably the directory that contains your image data, you need only to type

C:\NET> FTP

and access to Luthien is established. One may also connect to any other address in the internet by specifying a FTP address, just be sure to have a valid login account and a password. You can change directories in the FTP host by typing

FTP> cd directory

You can also change your local directory (say you want to transfer an image from another directory) by typing

FTP> \$cd directory

To copy a file to the FTP host, just type

FTP> put filename

Don't forget to change the data type to binary by typing

FTP> bin

at the FTP prompt or image files will not be transferred correctly and the computer will lock-up. You can transfer many files at once by typing

FTP> mput filenames

or by using the flag characters,? and *, to specify many filenames. The mput command stands for 'multiple put' and prompts the user at each filename to see if they want that file transferred or not. It is possible to disable this feature by typing

FTP> prompt

To quit FTP, just type

FTP> quit

A.2 PV-WAVE

PV-WAVE is a powerful, interactive command language, complete with all the program control options of a structured programming language. We currently have a single license so PV-WAVE is only available on Luthien and it is accessed, if unaliased, by typing

luthien: /usr/products/vni/wave/bin/wave

The manuals (5 thick ones!) are in the SPM lab.

PV-WAVE has a huge selection of functions to provide almost any data manipulation operation including:

Mathematical/Statistical Functions

Interpolation and Approximation

- Cubic spline interpolation
- Cubic spline evaluation and integration
- Spline interpolation
- Spline evaluation and integration
- Least squares approximation and smoothing
- Scattered data interpolation and approximation

Transforms

- One to eight dimensional Fast Fourier Transforms
- Chebyshev polynomials

Special Functions

- Error and gamma functions
- Bessel Functions
- Statistical probability distribution functions

Linear Systems

• Matrix inversion

- Linear equations with full matrices
- Linear least squares with full matrices

Eigensystem Analysis

- Linear eigensystems
- Generalized eigensystems

Quadrature

- Univariate quadrature
- Multivariate quadrature
- Gauss quadrature
- Numerical differentiation

Differential Equations

- Adams, Gear, or Runge-Kutta method
- Initial value problems

Nonlinear Equations

- Zeros of a polynomial
- Zeros of a function
- Roots of a system of equations

Optimization

. - .

- Unconstrained minimization
- Linearly constrained minimization
- Nonlinearly constrained minimization

Statistics and Random Number Generation

- Basic statistics
- Random numbers
- Correlation and regression
- Analysis of variance
- Time series and forecasting
- Multivariate analysis
- Probability distribution functions and inverses

Language and Graphics Functions

Animation

Array Manipulation

Color Table Manipulation

Communication with Databases

Device Handling

Files and Input/Output Functions

Image Display and Processing

Monitoring Multiple Concurrent Processes

Operating System Access

Plotting

- 2D
- 3D
- 4D
- Surface plots
- Contour plots
- Vector field plots
- Bar plots

Printing Functions

• Produces publication-quality output

Sting Processing

Utilities

- Set output files
- Time and date
- Error handling
- Constants

Variable Creation and Conversion

Window Creation and Manipulation

In addition to the built-in functions, you are able to write you own data manipulation procedures and call then in the main program. This is done by creating a file whose name ends in .pro. The file may contain a series of PV-WAVE commands and algorithms and is then called into the main program by simply typing the filename without the extension. For example, a function named SQUARE which calculates the square of a number has the filename square.pro and looks like this:

FUNCTION SQUARE, NUMBER RETURN, NUMBER^2 END

When the function is initially used in a PV-WAVE session, the file is automatically compiled. The result would look like this:

WAVE> x = square(10) & print, x % Compiled module: SQUARE 100

If you decide to change the source file after it has been compiled, you must recompile it with a .run or .rnew command.

The command language is not difficult to learn but it takes a little work to get your data to look the way you want.

A.3 SXM

SXM is a mouse driven shell written for PV-WAVE. Most commands we use frequently for image analysis are found here but it is possible to include your own functions if necessary. The commands are accessed by graphical menus where the mouse will highlight a function, the left mouse button will select that function, the right mouse button will bring up an options menu for that function, and the middle button will bring up a help window for that function.

Using SXM is pretty straightforward but you need a short guided tour to get familiar with the menu sequences. It is much simpler to use than PV-WAVE but you may not find the exact function you need.

A.4 Other Noise Sources

Although I dealt mostly with the vibration isolation as a noise source in the text, vibration is by no means the only culprit. The electronics and laser used in the microscope also contribute to the noise background. My colleagues Yanzhang Liu and Peter Grütter have optimized these to produce the greatest signal-to-noise ratio possible. Here is a brief description of some electronic noise sources. See Horowitz and Hill [89] and Sarid [94] for a more complete discussion of noise sources.

Johnson Noise

Thermal excitation of the electrons in a resistor generates a current noise known as Johnson Noise. The noise is 'white', meaning it has the same noise power at every frequency. The noise current of a resistor at temperature T is given by

$$I_{Johnson} = \sqrt{\frac{4k_BTB}{R}}$$

where B is the bandwidth in Hertz. We were able to minimize this noise source by substituting the $10k\Omega$ resistor in the laser pre-amplifier with a $20M\Omega$ resistor. Since the current from the photodetector is the same, and $I_{Johnson}$ wen down by a factor of 45, the signal-to-noise ratio went up considerably.

Shot Noise

Since an electric current is a flow of discrete charges, the finiteness of the charge quantum results in statistical fluctuations of the current. If charges act independently of each other, the fluctuating current is given by

$$I_{Shot} = \sqrt{2qI_{dc}B}$$

where q is the electronic charge, and I_{dc} is the "steady" current. The shot noise is white and becomes a significant portion of the current for small currents. For photodetectors, the noise varies as \sqrt{n} where n is the number of incident photons.

1/f Noise

Also known as flicker noise, 1/f noise is characterized by a large amplitude at low frequency that decays as the reciprocal of the frequency. This kind of noise is present in very many physical and electronic systems but its source is not well understood. Since the noise is a function of the frequency, this noise is known as 'pink'. In our detector, the 1/f noise may be caused by the hopping motion of impurities and defects in the path of the electrons.

Laser Intensity Noise

The dominant source of noise in a laser diode is spontaneous emission. The laser diode is actually an amplifier for this noise since it behaves as a thermal source. Also included are mode-hopping and 1/f noise of the laser. The junction temperature and drive current of the laser cause the center wavelength to shift. This causes what is known as "mode-hopping" as the laser switches from one longitudinal mode to another. Not only does the position of the mode change, but a temperature-dependent hysteresis can occur.

Laser Phase Noise

The fluctuations in the phase of an optical wave passing through an interferometer can be translated into intensity noise on a photodetector.

Bimorph Noise

The voltage noise on the terminals of the bimorph are translated into amplitude noise on the cantilever which is attached to it.

REFERENCES

- Albrecht, T. R., Akamine, S., Carver, T. E., and Quate, C. F. [90]. J. Vac. Sci. Technol., A8, 3386 (1990).
- Albrecht, T. R., Grütter, P., Horne, P., and Rugar, D. [91]. J. Appl. Phys., 69, 668 (1991).
- ALBRECHT, T. R., GRÜTTER, P., AND RUGAR, D. [92]. *Ultramicroscopy*, 42-44, 1638 (1992).
- ASHCROFT, N. AND MERMIN, D. [76]. Solid State Physics. W.B. Saunders Company, 1976.
- BARRETT, R. C. AND QUATE, C. F. [91]. Optical scan-correction system applied to atomic force microscopy. Submitted for Publication in Review of Scientific Instruments.
- Binning, G., Quate, C. F., and Gerber, C. [86]. Phys. Rev. Letters, 56, 930 (1986).
- Binning, G. and Rohrer, H. [82]. Helv. Phys. Acta, 55, 726 (1982).
- CHEN, G. Y., WARMACK, R. J., THUNDAT, T., ALLISON, D. P., AND HUANG, A. [94]. Rev. Sci. Instrum., 65, 2532 (1994).
- CUGAT, O., HANSSON, P., AND COEY, J. M. D. [94]. IEEE Transactions on Magnetics, 30, 4602 (1994).
- DREXLER, K. E. [91]. J. Vac. Sci. Technol., 9, 1394 (1991).
- FAROQUIT, M. M., EVANS, A. R., STEDMAN, M., AND HAYCOCKS, J. [92]. Nanotechnology, 3, 91 (1992).
- Fujisawa, S., Ohta, M., Konishi, T., Sugawara, Y., and Morita, S. [94]. Rev. Sci. Instrum., 65, 644 (1994).
- GRÜTTER, P. AND ALLENSPACH, R. [94]. Geophys. J. Int., 116, 502 (1994).
- Grütter, P., Mamin, H., and Rugar, D. Scanning Tunneling Microscopy II, volume 28, chapter 5. Springer-Verlag.
- GÜNTHERODT, H. J. AND WIESENDANGER, R., EDITORS [92]. Scanning Tunneling Microscopy I-III, volume 20, 28 and 29 of Springer Series in Surface Sciences. Springer-Verlag, 1992.
- HARTMANN, U. [91]. Phys. Rev. B, 43, 2404 (1991).

ζ,

- HOROWITZ, P. AND HILL, W. [89]. The Art of Electronics. Cambridge University Press, second edition, 1989.
- HOWLAND, R. S. [93]. How to buy a scanning probe microscope. Technical report, Park Scientific.
- HUTTER, J. L. AND BECHHOEFER, J. [93]. J. Appl. Phys., 73, 4123 (1993).

- ISRAELACHVILI, J. N. [91]. Intermolecular and Surface Forces. Academic Press, second edition, 1991.
- JORGENSEN, J. F., CARNEIRO, K., AND MADSEN, L. L. [93]. Hysteresis correction of scanning tunneling microscope images. Submitted for Publication in Journal of Vacuum Science and Technology B.
- MARTI, O. [93]. STM in Biology. McGraw-Hill, 1993.
- MEYER, E. [92]. Ultramicroscopy, 42-44, 274 (1992).
- MEYER, E. ET AL. [88]. J. Microscopy, 152, 269 (1988).
- OKANO, M., KAJIMURA, K., WAKIYAMA, S., SAKAI, F., MIZUTANI, W., AND ONO, M. [87]. J. Vac. Sci. Technol., A5, 3313 (1987).
- PARK, S.-I. AND QUATE, C. [87]. Rev. Sci. Instrum., 58, 2004 (1987).
- RUGAR, D. ET AL. [90]. J. Appl. Phys., 68, 1169 (1990).
- RUGAR, D., MAMIN, H. J., AND GUTHNER, P. [89]. Appl. Phys. Lett., 55, 2588 (1989).
- SARID, D. [94]. Scanning Force Microscopy. Oxford University Press, revised edition, 1994.
- SCHÖNENBERGER, C. AND ALVARADO, S. F. [90]. Z. Phys., 80, 373 (1990).
- TORTONESE, M. ET AL. [91]. Atomic force microscopy using piezoresistive cantilevers. In *Transducers '91*, 1991 International Conference on Solid-State Sensors and Actuators, 1991.
- ZÜGER, O., OTT, H. P., AND DÜRIG, U. [92]. Rev. Sci. Instrum., 63, 5634 (1992).